Dynamical spin structure factors of quantum spin nematic states

Ryuichi Shindou,[1,2] Seiji Yunoki,[3] and Tsutomu Momoi[2]

[1]*Physics Department, Tokyo Institute of Technology, Ookayama, 2-12-1, Meguro-ku, Tokyo Japan*
[2]*Condensed Matter Theory Laboratory, RIKEN, 2-1 Hirosawa, Wako, Saitama 351-0198, Japan*
[3]*Computational Condensed Matter Laboratory, RIKEN, 2-1 Hirosawa, Wako, Saitama 351-0198, Japan*

(Dated: September 30, 2011)

Dynamical spin structure factors of quantum spin nematic phase are studied using the large-N loop expansion in the spin-$\frac{1}{2}$ square-lattice J_1–J_2 model with ferromagnetic J_1 and competing antiferromagnetic J_2. As the starting mean-field state, we employ a spin-triplet pairing state of spinon fields, called Z_2 planar state, which was found as a large-N saddle point solution of the fermionic mean-field analysis [R. Shindou and T. Momoi, Phys. Rev. B **80**, 064410 (2009)]. Using the standard large-N expansion, we take into account the fluctuation within 1-loop level, which is equivalent to the random phase approximation. The spin structure factors thus obtained signifies the existence of the gapless k-linear spin-wave modes at $\boldsymbol{q} = (0, 0)$ and that at $\boldsymbol{q} = (0, \pi)$. The spectral weight of the former gapless modes vanish as linear functions of the momentum, while the latter mode has essentially no spectral weight in the dynamical spin structure factors. We also observed that the first gapped mode at $\boldsymbol{q} = (\pi, \pi)$, which can be observed in the longitudinal dynamical spin-structure factor, is a 'Higgs boson' associated with the Z_2 state. Namely, with decreasing J_2, the mass of the 'Higgs boson' vanishes at a critical value $J_2/J_1 = J_{c,2}$, so that the state reduces to the $U(1)$ planar state. We found that, when this happens, other gapped *magnetic* modes at $\boldsymbol{q} = (\pi, \pi)$ simultaneously exhibit instabilities. As a result, the $U(1)$ planar phase not only breaks the translational symmetries of the square lattice, but also it breaks a staggered $U(1)$ *spin*-rotational symmetry which is possessed by the Z_2 planar state.

PACS numbers:

I. INTRODUCTION

Frustrated magnets are Mott insulators where competing interactions among localized quantum spins bring about a large degeneracy in the ground state energetics. In a certain circumstance, such a frustrated spin system lifts this degeneracy quantum-mechanically, only to choose as its ground state a liquid-like magnetic state of matter, dubbed as a quantum spin liquid,[1], where the system does not exhibit any ordering down to the zero temperature.

The representative of quantum spin liquids is resonating valence bond (RVB) state in $S = \frac{1}{2}$ quantum spin systems,[2] whose building-block is the singlet valence bond, a pair of two $S = \frac{1}{2}$ spins forming the spin-singlet state. The wavefunction is given by an equally-weighted superposition of different spin-singlet dimer covering configurations, so that, unlike valence bond solid state or Neel state, the state preserves the lattice-translational symmetry. Owing to this fluid-like character of the ground-state wavefunction, quantum spin liquids have various exotic low-energy excitations, including emergent gauge fields, fractionalized magnetic excitations called spinons, and the topological degeneracy associated with this fractionalization.[1–4]

A new state of matter recently discussed in the localized spin systems is a quantum spin nematic state, which can be regarded as a quantum-spin analogue of nematic liquid crystals. It neither possesses spin order, i.e. sublattice magnetization, nor crystalline solid-like structure in spin degrees of freedom, but, unlike *spin-rotational symmetric* quantum spin liquids, it exhibits the spin nematic order measured by the rank-2 traceless tensor spin operator[5] $K_{\boldsymbol{jm},\mu\nu} \equiv S_{\boldsymbol{j},\mu} S_{\boldsymbol{m},\nu} - \frac{\delta_{\mu\nu}}{3} \langle \boldsymbol{S_j} \cdot \boldsymbol{S_m} \rangle$ for $\mu, \nu = 1, 2, 3$. The tensor is comprised by two distinct spin operators defined on different sites, usually neighboring two sites, so that the tensor is introduced on the bond. The state is thereby called as the 'bond-type' spin nematic state. Depending on the symmetry under the exchange of spin indices, $\mu \leftrightarrow \nu$, quantum spin nematics can be classified into two categories:[5] the chiral type (p-nematic) and the non-chiral type (n-nematic). The order parameter of the former one is the vector chirality defined as $\langle \boldsymbol{S_j} \times \boldsymbol{S_m} \rangle$, while that of the latter is the symmetric part of the quadratic tensor, $\langle Q_{\boldsymbol{jm},\mu\nu} \rangle = \frac{1}{2} \langle K_{\boldsymbol{jm},\mu\nu} + K_{\boldsymbol{jm},\nu\mu} \rangle$.

A p-nematic state was first introduced as a *helical* quantum spin liquid in a frustrated antiferromagnetic Heisenberg model by Chandra, Coleman and Larkin.[6] The state essentially acquires a linear combination of the spin-*triplet* valence bond and singlet valence bond on the same bond, i.e. $|\uparrow\downarrow\rangle + e^{i\phi} |\downarrow\uparrow\rangle$, which induces a finite vector chirality on the bond. Meanwhile, possible realization of n-nematic states has been investigated recently in various quantum frustrated *ferromagnetic* Heisenberg models,[7–11] where dynamics of (purely) spin-triplet valence bonds brings about the long range ordering of the symmetric order parameter $\langle Q_{\boldsymbol{jm},\mu\nu} \rangle$. Both of these bond-type spin nematic states preserve the translational symmetries of the original lattices, so that they can be regarded as a 'cousin' of symmetric quantum spin liquids, sharing many of their exotic aspects.

Motivated by these recent findings, the present authors

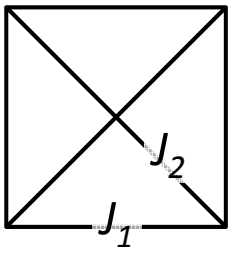

FIG. 1: Square lattice J_1-J_2 frustrated ferromagnetic model, where the nearest neighbor exchange J_1 is ferromagnetic and the next nearest neighbor exchange J_2 is antiferromagnetic.

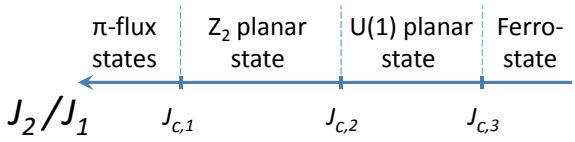

FIG. 2: Phase diagram of the square lattice J_1-J_2 model in the large-N limit. The nearest neighbor exchange J_1 is ferromagnetic and the next nearest neighbor exchange J_2 is antiferromagnetic. Energetics of the mean-field solutions conclude that $J_{c,1} = 1.325$, $J_{c,2} = 1.0448$ and $J_{c,3} = 1.02$.

formulated the mean-field theory of bond-type spin nematic states in spin-$\frac{1}{2}$ spin systems in terms of fermion representation, where the spin-triplet pairing of spinon fields describes the spin-triplet valence bond.[10] It turns out that the so-called d-vector associated with this triplet pairing function mimics the director vector in the n-nematics, while the product between the d-vector and singlet pairing amplitude defines the vector chirality associated with the p-nematics. Using this formulation, we derived the mean-field phase diagram of the square lattice J_1-J_2 model with ferromagnetic (FM) J_1 and competing antiferromagnetic (AF) J_2, thereby finding that a certain spin triplet pairing state, dubbed as the Z_2 planar state,[12] is most energetically favorable when competition between the FM J_1 and the AF J_2 interactions is strong (see Fig. 2). The variational Monte Carlo (VMC) study based on this mean-field analysis further indicated that, when projected onto the physical spin Hilbert space, the BCS wavefunction constructed from the Z_2 planar state achieves the best optimal energy, compared with other competing states such as the ferromagnetic state and the collinear antiferromagnetic state.[13] This projected Z_2 planar state possesses the same 'd-wave' spatial configuration of the bond quadrupole order[10,13] as suggested by the previous exact diagonalization study.[9]

In this paper, we theoretically investigate the nature of low-energy magnetic excitations in the quantum spin nematic state. We calculate the dynamical magnetic properties of the Z_2 planar state, so as to give relevant physical characterizations to the bond-type spin nematic phase. Specifically, using a standard large-N loop expansion, we take into account the fluctuation around the mean-field state within the one-loop level. This treatment essentially corresponds to the random phase approximation (RPA). The spin structure factor thus obtained has two aspects; spin-liquid like character and spontaneously symmetry breaking (SSB) phase character. The former feature manifests itself as the Stoner continuum of the individual excitations of gapped free spinons. On the one hand, the SSB phase character is represented by the gapless spin-wave modes, which have linear energy dispersions and whose spectral weight vanishes as a linear function of the momentum near the gapless point.

When the antiferromagnetic coupling J_2 decreases, the mean-field solution transforms from the Z_2 planar state to the $U(1)$ planar state at $J_2/J_1 = J_{c,2}$ (see Fig. 2). Namely, previous field-theoretical analysis suggested that, some of the gapped gauge bosons in the Z_2 planar state become gapless at the transition point, only to constitute a compact QED (quantum electrodynamics) action for $J_2/J_1 < J_{c,2}$, where the space-time instanton effect associated with this effective action introduces a strong confining potential between 'free' gapped spinons. Throughout the RPA calculation in this paper, we found that the first gapped modes at $\boldsymbol{q} = (\pi, \pi)$ are actually these gapped gauge bosons, whose finite mass therefore quantifies the stability of the Z_2 planar state against the confinement effect. We also found that, when the Z_2 state is transformed into the $U(1)$ state, two *other* magnetic modes at the same zone boundary point *simultaneously* exhibit the instability. As a result, the $U(1)$ planar phase breaks the translational symmetries and also a certain type of the *spin*-rotational symmetry.

The organization of this paper is as follows: In the next section, we first introduce a 'general-N' quantum frustrated ferromagnetic model, whose large-N limit possesses our previous mean-field solutions as the 'exact' ground states and whose $N = 1$ case safely reproduces the usual quantum spin-$\frac{1}{2}$ model. In Sec. III, we will describe the $\frac{1}{N}$-expansion calculation for the dynamical spin-spin correlation functions. In Sec. IV, we show the calculated dynamical spin structure factors, both longitudinal and transverse, and discuss their characteristic features and its physical implications. We also discuss about the nature of the $U(1)$ planar state here. Section V is devoted to the summary and discussion.

II. QUANTUM FRUSTRATED FERROMAGNETIC MODEL

In this section, we will briefly review the Z_2 planar state as a saddle point solution in the large-N limit of a 'general-N' quantum frustrated ferromagnetic model.

The large-N model is given by[10]

$$\mathcal{H} = -\frac{J_1}{N}\sum_{\langle \boldsymbol{j},\boldsymbol{m}\rangle}\sum_{a,b=1}^{N}\{\boldsymbol{S}^{ab}_{\boldsymbol{j}}\cdot\boldsymbol{S}^{ba}_{\boldsymbol{m}}+\psi^{ab}_{\boldsymbol{j}}\psi^{ba}_{\boldsymbol{m}}\} + \frac{J_2}{N}\sum_{\langle\langle \boldsymbol{j},\boldsymbol{m}\rangle\rangle}\sum_{a,b}\boldsymbol{S}^{ab}_{\boldsymbol{j}}\cdot\boldsymbol{S}^{ba}_{\boldsymbol{m}}+\sum_{\boldsymbol{j},a}\boldsymbol{h}^{aa}_{\boldsymbol{j}}\cdot\boldsymbol{S}^{aa}_{\boldsymbol{j}}, \quad (1)$$

where $\langle \boldsymbol{j},\boldsymbol{m}\rangle$ ($\langle\langle \boldsymbol{j},\boldsymbol{m}\rangle\rangle$) runs over all nearest-neighbor (2nd-neighbor) bonds on the square lattice and

$$\begin{aligned} S^{ab}_{\boldsymbol{j},+} &\equiv \frac{1}{2}\big(f^{a\dagger}_{\boldsymbol{j},\uparrow}f^{b}_{\boldsymbol{j},\downarrow}+f^{b\dagger}_{\boldsymbol{j},\uparrow}f^{a}_{\boldsymbol{j},\downarrow}\big),\\ S^{ab}_{\boldsymbol{j},-} &\equiv \frac{1}{2}\big(f^{a\dagger}_{\boldsymbol{j},\downarrow}f^{b}_{\boldsymbol{j},\uparrow}+f^{b\dagger}_{\boldsymbol{j},\downarrow}f^{a}_{\boldsymbol{j},\uparrow}\big),\\ S^{ab}_{\boldsymbol{j},3} &\equiv \frac{1}{2}\big(f^{a\dagger}_{\boldsymbol{j},\uparrow}f^{b}_{\boldsymbol{j},\uparrow}-f^{b\dagger}_{j,\downarrow}f^{a}_{j,\downarrow}\big),\\ \psi^{ab}_{\boldsymbol{j}} &\equiv \frac{i}{2}\big(f^{a\dagger}_{\boldsymbol{j},\alpha}f^{b}_{\boldsymbol{j},\alpha}-f^{b\dagger}_{\boldsymbol{j},\alpha}f^{a}_{\boldsymbol{j},\alpha}\big). \end{aligned} \quad (2)$$

Here $f^{a\dagger}_{\boldsymbol{j},\alpha}$ is a fermion creation operator with spin $\alpha =\uparrow$ or $\downarrow$ and flavor $a = 1,\ldots,N$. In this paper, we consider the case J_1 is ferromagnetic and J_2 is antiferromagnetic, i.e. $J_1, J_2 > 0$. We have introduced an external magnetic field $\boldsymbol{h}^{aa}_{\boldsymbol{j}}$ to calculate the spin-spin correlation function. The physical spin Hilbert space satisfies the constraint

$$\sum_{a=1}^{N}f^{a\dagger}_{\boldsymbol{j},\alpha}f^{a}_{\boldsymbol{j},\alpha}=N, \quad \sum_{a=1}^{N}f^{a}_{\boldsymbol{j},\alpha}f^{a}_{\boldsymbol{j},\beta}\epsilon_{\alpha\beta}=0 \quad (3)$$

on every site $\boldsymbol{j}$. When $N = 1$, Eq. (1) in the physical Hilbert space reduces to the usual J_1-J_2 quantum Heisenberg model with spin-$\frac{1}{2}$. We regard N to be large when we perform the $1/N$ loop-expansion.

An equivalent statistical-mechanics problem at temperature β^{-1} can be formulated in terms of the path-integral,

$$Z[h] = \int \mathcal{D}\Psi^{a\dagger}\mathcal{D}\Psi^{a}\mathcal{D}\boldsymbol{a}_\tau\mathcal{D}U^{\rm sin}\mathcal{D}\boldsymbol{U}^{\rm tri} \exp\left(-\int_0^\beta d\tau\,\mathcal{L}[h,U^{\rm sin},\boldsymbol{U}^{\rm tri},\boldsymbol{a}_\tau]\right),$$

and

$$\begin{aligned}\mathcal{L} = \sum_{a=1}^{N}\Bigg\{&\frac{1}{2}\sum_{\boldsymbol{j}}\mathrm{tr}\Big[\Psi^{a\dagger}_{\boldsymbol{j}}\big(\partial_\tau+\sum_{\nu=1}^{3}ia^{\nu}_{\boldsymbol{j},\tau}\sigma_\nu\big)\Psi^{a}_{\boldsymbol{j}}\Big]\\ &-\frac{J_1}{4}\sum_{\langle j,m\rangle}\Big(-|\boldsymbol{E}_{\boldsymbol{jm}}|^2-|\boldsymbol{D}_{\boldsymbol{jm}}|^2+\mathrm{tr}\big[\Psi^{a\dagger}_{\boldsymbol{j}}U^{\rm tri}_{\boldsymbol{jm},\mu}\Psi^{a}_{\boldsymbol{m}}\sigma^{T}_{\mu}\big]\Big)\\ &-\frac{J_2}{4}\sum_{\langle\langle \boldsymbol{j},\boldsymbol{m}\rangle\rangle}\Big(-|\chi_{\boldsymbol{jm}}|^2-|\eta_{\boldsymbol{jm}}|^2+\mathrm{tr}\big[\Psi^{a\dagger}_{\boldsymbol{j}}U^{\rm sin}_{\boldsymbol{jm}}\Psi^{a}_{\boldsymbol{m}}\big]\Big)\\ &+\frac{1}{4}\sum_{\boldsymbol{j}}\sum_{\mu=1}^{3}h^{aa}_{\boldsymbol{j},\mu}\,\mathrm{tr}\big[\Psi^{a\dagger}_{\boldsymbol{j}}\Psi^{a}_{\boldsymbol{j}}\sigma^{T}_{\mu}\big]\Bigg\}, \end{aligned} \quad (4)$$

where the fermion field is written in the 2×2 matrix form

$$\Psi^{a\dagger}_{\boldsymbol{j}}\equiv\begin{bmatrix} f^{a\dagger}_{\boldsymbol{j},\uparrow} & f^{a}_{\boldsymbol{j},\downarrow}\\ f^{a\dagger}_{\boldsymbol{j},\downarrow} & -f^{a}_{\boldsymbol{j},\uparrow}\end{bmatrix} \quad (5)$$

and the auxiliary fields are written as

$$\hat{U}^{\rm sin}_{\boldsymbol{jm}}\equiv\begin{bmatrix}\chi^{*}_{jm} & \eta^{*}_{\boldsymbol{jm}}\\ \eta_{\boldsymbol{jm}} & -\chi_{\boldsymbol{jm}}\end{bmatrix},\quad \hat{U}^{\rm tri}_{\boldsymbol{jm},\mu}\equiv\begin{bmatrix}E^{*}_{\boldsymbol{jm},\mu} & D^{*}_{\boldsymbol{jm},\mu}\\ -D_{\boldsymbol{jm},\mu} & E_{\boldsymbol{jm},\mu}\end{bmatrix} \quad (6)$$

($\mu = 1,2,3$). The trace denoted by the symbol "tr" is taken over 2×2 matrices such as $\Psi^{a}_{\boldsymbol{j}}$ and the Pauli matrices σ_μ. Integrating over the temporal gauge fields $\boldsymbol{a}_{\boldsymbol{j},\tau}$ strictly imposes the local constraints given by Eq. (3) on every site and time. In this formulation, the ferromagnetic exchange interaction was decoupled in terms of spin-triplet pairing fields and spin-triplet hopping fields

$$D_{\boldsymbol{jl},\mu}\equiv i\langle f_{\boldsymbol{j},\alpha}[\sigma_2\sigma_\mu]_{\alpha\beta}f_{\boldsymbol{l},\beta}\rangle,\quad E_{\boldsymbol{jl},\mu}\equiv\langle f^{\dagger}_{\boldsymbol{j},\alpha}[\sigma_\mu]_{\alpha\beta}f_{\boldsymbol{l},\beta}\rangle, \quad (7)$$

while antiferromagnetic one was decomposed into the spin-singlet pairing and hopping fields

$$\eta_{\boldsymbol{jl}}\equiv-i\langle f_{\boldsymbol{j},\alpha}[\sigma_2]_{\alpha\beta}f_{\boldsymbol{l},\beta}\rangle,\quad \chi_{\boldsymbol{jl}}\equiv\langle f^{\dagger}_{\boldsymbol{j},\alpha}f_{\boldsymbol{l},\alpha}\rangle. \quad (8)$$

A Gaussian-integral over these auxiliary fields reproduces the original Hamiltonian given in Eq. (1).

We can formally rewrite the effective action as

$$\int_0^\beta d\tau\mathcal{L}=N\mathcal{S}_{\rm I} + \frac{1}{2}\sum_{\boldsymbol{k},n,a}\boldsymbol{f}^{\dagger}_{\boldsymbol{k},n,a}\cdot\boldsymbol{G}^{-1}_{(\boldsymbol{k},n|\boldsymbol{k}',n')}[h^{aa},U^{\rm sin},U^{\rm tri},\boldsymbol{a}_\tau]\cdot\boldsymbol{f}_{\boldsymbol{k}',n',a}, \quad (9)$$

introducing the Nambu representation of the fermion field

$$\boldsymbol{f}^{\dagger}_{\boldsymbol{k},n,a}\equiv\begin{pmatrix} f^{a\dagger}_{\boldsymbol{k},n,\uparrow} & f^{a\dagger}_{\boldsymbol{k},n,\downarrow} & f^{a}_{-\boldsymbol{k},-n,\uparrow} & f^{a}_{-\boldsymbol{k},-n,\downarrow}\end{pmatrix} \quad (10)$$

with

$$f^{a\dagger}_{\boldsymbol{k},n,\sigma}\equiv\frac{1}{\sqrt{\beta N_\Lambda}}\sum_{\boldsymbol{j}}\int_0^\beta d\tau\,e^{i\boldsymbol{k}\cdot\boldsymbol{j}+i\omega_n\tau}f^{a\dagger}_{\boldsymbol{j},\sigma}(\tau), \quad (11)$$

where N_Λ denotes the total number of lattice site and $\omega_n\equiv(2n+1)\pi\beta^{-1}$. In Eq. (9),

$$\mathcal{S}_{\rm I}\equiv\int_0^\beta d\tau\Big\{\frac{J_1}{4}\sum_{\langle \boldsymbol{j},\boldsymbol{m}\rangle}\big(|\boldsymbol{E}_{\boldsymbol{jm}}|+|\boldsymbol{D}_{\boldsymbol{jm}}|\big) + \frac{J_2}{4}\sum_{\langle\langle \boldsymbol{j},\boldsymbol{m}\rangle\rangle}\big(|\chi_{\boldsymbol{jm}}|+|\eta_{\boldsymbol{jm}}|\big)\Big\} \quad (12)$$

and $\boldsymbol{G}^{-1}$ denotes the inverse of a single-particle Green function of the fermion field. Integral over the Ψ ($\boldsymbol{f}$)

fields in Eq. (4) leads to the following partition function,

$$Z[h] = \int \mathcal{D}U^{\rm sin}\mathcal{D}\boldsymbol{U}^{\rm tri}\mathcal{D}\boldsymbol{a}_\tau \exp\big[-N\mathcal{S}[h, U^{\rm sin}, U^{\rm tri}, \boldsymbol{a}_\tau]\big], \tag{13}$$

$$\mathcal{S} \equiv \mathcal{S}_{\rm I} + \mathcal{S}_{\rm II} \tag{14}$$

$$\mathcal{S}_{\rm II} \equiv -\frac{1}{2N}\sum_{a=1}^{N}{\rm Tr}\big(\ln \boldsymbol{G}^{-1}[h^{aa}, U^{\rm sin}, U^{\rm tri}, \boldsymbol{a}_\tau]\big). \tag{15}$$

where the Green function $\boldsymbol{G}$ is diagonal in the flavor index. The trace of $\ln \boldsymbol{G}^{-1}$ is taken over the momentum ($\boldsymbol{k}$), the Matsubara frequency (ω_n), spin index (σ), and particle-hole index.

$\mathcal{S}_{\rm II}$ as well as $\mathcal{S}_{\rm I}$ are at most on the order of unit in large-N limit, and the same is for $\mathcal{S}$. Hence, in this limit, we can evaluate the partition function, substituting the saddle point solution of the action given by

$$\frac{\delta\mathcal{S}}{\delta U^{\rm sin}} = \frac{\delta\mathcal{S}}{\delta U^{\rm tri}} = \frac{\delta\mathcal{S}}{\delta \boldsymbol{a}_\tau} = 0. \tag{16}$$

The present authors previously investigated various local minima of the action at zero magnetic field, $h = 0$, by assuming that $U^{\rm sin}$, $U^{\rm tri}$ and $\boldsymbol{a}_\tau$ thus determined are temporally uniform and also preserve the translational symmetries of the bsquare lattice. Throughout this study, we found that, in the intermediate coupling region, the saddle point solution acquires a finite spin-triplet pairing on every ferromagnetic bonds, while singlet pairings on the antiferromagnetic bonds.

In particular, when the next nearest neighbor antiferromagnetic exchange interaction supports the 'π-flux'-type singlet pairings, a coplanar configuration of the spin-triplet d-vectors on the ferromagnetic interactions realizes the 'best' mean-field energy among the others.[10] This mean-field solution, which we call 'Z_2 planar state', is given by

$$\begin{aligned}&\bar{U}^{\rm tri}_{\langle \boldsymbol{j}, \boldsymbol{j}+\boldsymbol{e}_x\rangle,\mu} \equiv i\delta_{\mu,1}D\sigma_2, \quad \bar{U}^{\rm tri}_{\langle \boldsymbol{j}, \boldsymbol{j}+\boldsymbol{e}_y\rangle,\mu} \equiv i\delta_{\mu,2}D\sigma_2,\\ &\bar{U}^{\rm sin}_{\langle \boldsymbol{j}, \boldsymbol{j}+\boldsymbol{e}_x\pm\boldsymbol{e}_y\rangle} \equiv \chi\sigma_3 \pm \eta\sigma_1, \quad \bar{a}^{\mu}_{\boldsymbol{j},\tau} = 0,\end{aligned} \tag{17}$$

with $\boldsymbol{j} = (j_x, j_y)$, $\boldsymbol{e}_x = (1, 0)$ and $\boldsymbol{e}_y = (0, 1)$. The invariant gauge group of this mean-field state dictates that all the gauge excitations around this mean-field solution have finite gap [are not required to be gapless by the local $SU(2)$ gauge symmetry]. The state has the same spin-triplet pairing function as a 'planar' type superfluid B-phase ^{3}He: it is thereby dubbed as the 'Z_2 planar state'. Though the coplanar ordering of the $\boldsymbol{d}$-vectors breaks the $SU(2)$ spin-rotational symmetries completely, this ordering also endows the state with a *staggered* $U(1)$ spin-rotational symmetry. That is, the state defined by Eq. (17) is invariant under the following rotation in the spin-space,

$$\Psi^\dagger_{\boldsymbol{j}} \to e^{i(-1)^{j_x+j_y}\theta\sigma_3}\Psi^\dagger_{\boldsymbol{j}}, \quad \Psi_{\boldsymbol{j}} \to \Psi_{\boldsymbol{j}}e^{i(-1)^{j_x+j_y}\theta\sigma_3}, \tag{18}$$

for any θ, where the rotational axis is perpendicular to the coplanar plane.

The variational Monte Carlo study further indicates that the projected BCS wavefunction constructed from this Z_2 planar state achieves the best optimal energy in the range $0.42J_1 \le J_2 \le 0.57J_1$ in intermediate coupling regime, when compared with energies of other competing phases such as ferromagnetic state and collinear Neel state.[13] Moreover, the projected BCS wavefunction belongs to the same space group (including its irreducible representation)[13] as that of a bond-type spin nematic phase suggested by the exact diagonalization (ED) study in the same parameter region. The spin-spin correlation function calculated with respect to this projected BCS wavefunction exhibits a similar behavior[13] as those obtained from the ED studies up to 40 sites.[14] Observing these consistencies with the previous ED results including its energetics, we regard that this projected Z_2 planar phase is indeed realized as a bond-type spin nematic phase within a certain range of the intermediate coupling regime of the present J_1-J_2 spin model. Based on this assumption, we start from the mean-field Z_2 planar state, only to derive the dynamical magnetic properties of this bond-type spin nematic phase.

In the momentum representation, the Bogoliubov–de Gennes Hamiltonian for this Z_2 planar state is given by $\mathcal{H}_{\rm BdG} = \sum_{\boldsymbol{k},a}\boldsymbol{f}^{a\dagger}_{\boldsymbol{k}}\boldsymbol{H}^{(0)}_{\boldsymbol{k}}\boldsymbol{f}^{a}_{\boldsymbol{k}}$ and

$$\boldsymbol{H}^{(0)}_{\boldsymbol{k}} \equiv \frac{J_1 D}{2}s_x\boldsymbol{\gamma}_3 - \frac{J_1 D}{2}s_y\boldsymbol{\gamma}_5 + J_2\chi c_x c_y\boldsymbol{\gamma}_4 + J_2\eta s_x s_y\boldsymbol{\gamma}_2, \tag{19}$$

with $s_\mu \equiv \sin k_\mu$ and $c_\mu \equiv \cos k_\mu$. The 4×4 γ-matrices are defined as

$$\gamma_1 = \sigma_2 \otimes \sigma_1 = \begin{pmatrix} 0 & -i\sigma_1 \\ i\sigma_1 & 0 \end{pmatrix}, \tag{20}$$

where the 2×2 Pauli matrices σ_μ ($\mu = 1, 2, 3$) in front of the $\otimes$-mark is for the particle-hole space, while the other is for the spin space. Using the same notation, we define the other 4 anti-commutating γ-matrices as $\gamma_2 = \sigma_2\otimes\sigma_2$, $\gamma_3 = \sigma_2 \otimes \sigma_3$, $\gamma_4 = \sigma_3 \otimes \sigma_0$, $\gamma_5 = \sigma_1 \otimes \sigma_0$.

At this saddle point, the partition function is evaluated as

$$Z^{(0)}[h] = \exp\Big(-N\mathcal{S}^{(0)}[h]\Big), \tag{21}$$

$$\mathcal{S}^{(0)}[h] = \mathcal{S}^{(0)}_{\rm I} + \mathcal{S}^{(0)}_{\rm II}[h], \tag{22}$$

$$\mathcal{S}^{(0)}_{\rm I} = \frac{\beta}{2}\Big\{J_1 N_\Lambda D^2 + J_2 N_\Lambda\big(\chi^2 + \eta^2\big)\Big\}, \tag{23}$$

$$\mathcal{S}^{(0)}_{\rm II}[h] = -\frac{1}{2N}\sum_{a=1}^{N}{\rm Tr}\Big(\ln \boldsymbol{G}^{-1}_0[h^{aa}]\Big), \tag{24}$$

where the trace is over the momentum ($\boldsymbol{k}$), the Matsubara frequency (n), spin, and particle-hole indices. The single-particle Green function at the saddle point, $\boldsymbol{G}_0$, is

given by

$$G^{-1}_{0,(\boldsymbol{k},n,a|\boldsymbol{k}',n',a)}[h] \equiv \delta_{n,n'}\delta_{\boldsymbol{k},\boldsymbol{k}'} g_0^{-1}(\boldsymbol{k}, i\omega_n) + \frac{1}{2}\frac{1}{\sqrt{\beta N_\Lambda}} \sum_{\mu=1}^{3}\sum_{\boldsymbol{q},m} \delta_{\boldsymbol{k},\boldsymbol{k}'+\boldsymbol{q}}\delta_{n,n'+m}\, h^{aa}_{\boldsymbol{q},m,\mu}\boldsymbol{u}_\mu, \quad (25)$$

$$g_0^{-1}(\boldsymbol{k}, i\omega_n) = i\omega_n \boldsymbol{\gamma}_0 - \boldsymbol{H}^{(0)}_{\boldsymbol{k}}, \quad (26)$$

where the bosonic fields are Fourier-transformed as

$$h^{aa}_{\boldsymbol{q},m,\mu} \equiv \frac{1}{\sqrt{\beta N_\Lambda}} \sum_{\boldsymbol{j}} \int_0^\beta d\tau\, e^{-i\boldsymbol{q}\cdot\boldsymbol{j} - i\epsilon_m \tau} h^{aa}_{\boldsymbol{j},\mu}(\tau) \quad (27)$$

with $\epsilon_m \equiv 2m\pi\beta^{-1}$. The 4×4 Hermite matrices $\boldsymbol{u}_\mu$ ($\mu = 1, 2, 3$) are defined as follows:

$$\boldsymbol{u}_1 \equiv \boldsymbol{\gamma}_{15} = -i\boldsymbol{\gamma}_1\boldsymbol{\gamma}_5, \quad \boldsymbol{u}_2 \equiv \boldsymbol{\gamma}_{13} = -i\boldsymbol{\gamma}_1\boldsymbol{\gamma}_3, \quad \boldsymbol{u}_3 \equiv \boldsymbol{\gamma}_{35} = -i\boldsymbol{\gamma}_3\boldsymbol{\gamma}_5. \quad (28)$$

III. LOOP EXPANSION FOR CORRELATION FUNCTIONS

In the previous section, we have introduced the Z_2 planar state as the saddle point solution of the general-N quantum frustrated ferromagnetic model. Starting from this saddle point solution, we will calculate in this section the spin-spin correlation function, including the effect of the fluctuation of the auxiliary fields and the gauge fields around the local minimum within the random phase approximation (RPA). Specifically, from the saddle point solution, we first obtain the Hartree-Fock contribution to the spin-spin correlation functions. We next give a symbolic expression for the spin-spin correlation function, which includes the arbitrary order of the quantum corrections to this Hartree-Fock contribution. Based on this expression, we finally perform $1/N$ expansion and calculate the first order quantum correction of $\mathcal{O}(N)$, which corresponds to the random phase approximation term.

Derivatives of the partition function $Z[h]$ [Eq. (13)] in external fields generate spin-spin correlation functions,[15]

$$C^{aa}_{\mu\nu}(\boldsymbol{j},\tau) \equiv \langle \mathcal{T}\{\boldsymbol{S}^{aa}_{\boldsymbol{0},\mu}(0)\boldsymbol{S}^{aa}_{\boldsymbol{j},\nu}(\tau)\}\rangle|_{h=0} = C^{aa}_{\mu\nu,\mathrm{I}}(\boldsymbol{j},\tau) + C^{aa}_{\mu\nu,\mathrm{II}}(\boldsymbol{j},\tau) \quad (29)$$

with

$$C^{aa}_{\mu\nu,\mathrm{I}}(\boldsymbol{j},\tau) = -\frac{N}{Z}\int \mathcal{D}U^{\mathrm{sin}}\mathcal{D}\boldsymbol{U}^{\mathrm{tri}}\mathcal{D}\boldsymbol{a}_\tau \frac{\partial^2\mathcal{S}}{\partial h^{aa}_{\boldsymbol{0},\mu}(0)\partial h^{aa}_{\boldsymbol{j},\nu}(\tau)} \exp\big[-N\mathcal{S}\big]\Big|_{h=0}, \quad (30)$$

$$C^{aa}_{\mu\nu,\mathrm{II}}(\boldsymbol{j},\tau) = \frac{N^2}{Z}\int \mathcal{D}U^{\mathrm{sin}}\mathcal{D}\boldsymbol{U}^{\mathrm{tri}}\mathcal{D}\boldsymbol{a}_\tau \frac{\partial\mathcal{S}}{\partial h^{aa}_{\boldsymbol{0},\mu}(0)}\frac{\partial\mathcal{S}}{\partial h^{aa}_{\boldsymbol{j},\nu}(\tau)} \exp\big[-N\mathcal{S}\big]\Big|_{h=0}. \quad (31)$$

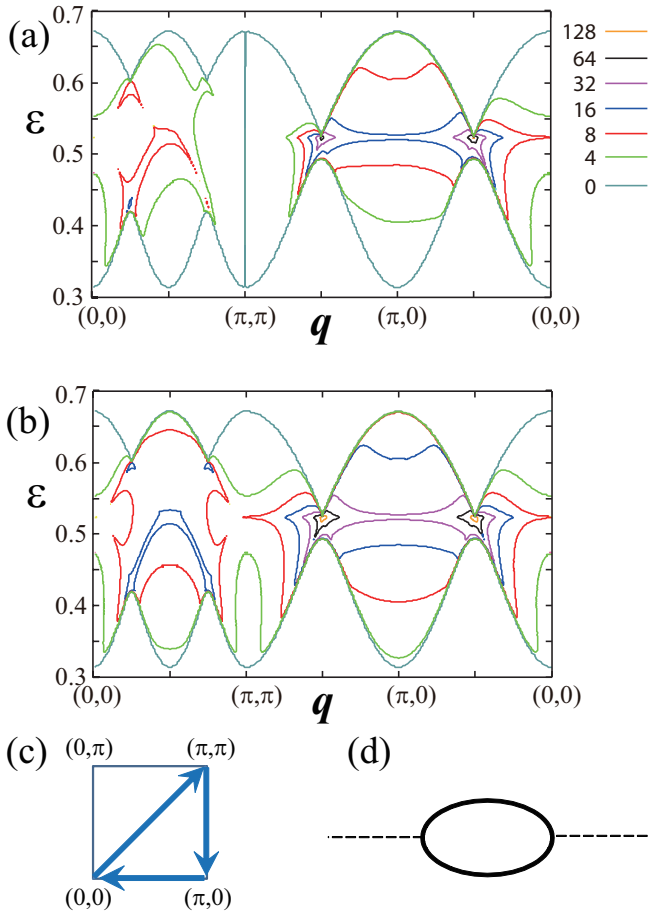

FIG. 3: A contour-plot of (a) $\mathrm{Im}\chi^{(0)}_{zz}(\boldsymbol{q},\epsilon)$ and (b) $\mathrm{Im}\chi^{(0)}_{+-}(\boldsymbol{q},\epsilon)$ at $J_2 = 1.1J_1$. The momentum $\boldsymbol{q}$ runs from $(0,0)$ to (π,π), to $(\pi,0)$ and back to the Γ-point (see Fig. (c)). Both of them have finite weight only at $\epsilon \geq \omega_c$, where $\omega_c \simeq 0.3$. (d) Feynman diagram for $\mathrm{Im}\chi^{(0)}_{\mu\mu}$.

where we do *not* take the summation over the flavor index 'a'. The imaginary-time ordered correlation function, $C_{\mu\mu}(\boldsymbol{j},\tau)$, is related to the real time dynamical susceptibility, $\chi_{\mu\mu}(\boldsymbol{q},\epsilon) \equiv \chi_{\mu\mu}(\boldsymbol{q}, i\epsilon_m = \epsilon + i\delta)$, in the form

$$\chi^{aa}_{\mu\mu}(\boldsymbol{q}, i\epsilon_m) = \sum_{\boldsymbol{j}}\int_0^\beta d\tau\, e^{-i(\boldsymbol{q}\cdot\boldsymbol{j}+\epsilon_m\tau)} C^{aa}_{\mu\mu}(\boldsymbol{j},\tau). \quad (32)$$

If we omit the fluctuations around the saddle point solution, we obtain the Hartree-Fock contribution to the correlation function,

$$C^{aa,(0)}_{\mu\nu}(\boldsymbol{j},\tau) = \frac{e^{-N\mathcal{S}^{(0)}}}{Z^{(0)}}\left\{-N\frac{\partial^2\mathcal{S}^{(0)}}{\partial h^{aa}_{\boldsymbol{0},\mu}(0)\partial h^{aa}_{\boldsymbol{j},\nu}(\tau)} + N^2\frac{\partial\mathcal{S}^{(0)}}{\partial h^{aa}_{\boldsymbol{0},\mu}(0)}\frac{\partial\mathcal{S}^{(0)}}{\partial h^{aa}_{\boldsymbol{j},\nu}(\tau)}\right\}\Big|_{h=0}. \quad (33)$$

Or equivalently,

$$\begin{aligned}
&\chi^{aa,(0)}_{\mu\nu}(\boldsymbol{q}, i\epsilon_m)\\
=&\frac{1}{8\beta N_\Lambda}\sum_{\boldsymbol{k},n}\mathrm{Tr}\big[\boldsymbol{g}_0(\boldsymbol{k}+\boldsymbol{q}, i\omega_n+i\epsilon_m)\,\boldsymbol{u}_\mu\,\boldsymbol{g}_0(\boldsymbol{k}, i\omega_n)\,\boldsymbol{u}_\nu\big]\\
&+\frac{\delta_{\boldsymbol{q},\boldsymbol{0}}\delta_{m,0}}{16\beta N_\Lambda}\Big(\sum_{\boldsymbol{k},n}\mathrm{Tr}\big[\boldsymbol{g}_0(\boldsymbol{k}, i\omega_n)\,\boldsymbol{u}_\mu\big]\Big)\\
&\qquad\times\Big(\sum_{\boldsymbol{k}',n'}\mathrm{Tr}\big[\boldsymbol{g}_0(\boldsymbol{k}', i\omega_{n'})\,\boldsymbol{u}_\nu\big]\Big),
\end{aligned}\tag{34}$$

where the trace in Eq. (34) is over the spin index and particle-hole index. From Eqs. (26,19,28), it is clear that $\boldsymbol{g}_0(\boldsymbol{k}, i\omega_n)\,\boldsymbol{u}_\mu$ is traceless for any $\mu = 1, 2, 3$. Thus, we can omit the second term as

$$\begin{aligned}
&\chi^{aa,(0)}_{\mu\nu}(\boldsymbol{q}, i\epsilon_m)\\
=&\frac{1}{8\beta N_\Lambda}\sum_{\boldsymbol{k},n}\mathrm{Tr}\big[\boldsymbol{g}_0(\boldsymbol{k}+\boldsymbol{q}, i\omega_n+i\epsilon_m)\boldsymbol{u}_\mu\,\boldsymbol{g}_0(\boldsymbol{k}, i\omega_n)\boldsymbol{u}_\nu\big].
\end{aligned}\tag{35}$$

The Hartree-Fock solution Eq. (35) brings about only the so-called Stoner continuum, which stems from *individual* excitations of the 'free' neutral fermions (spinons). After the analytic continuation, $i\epsilon_n \to \epsilon + i\delta$, we obtain the real-time dynamical susceptibilities, whose imaginary parts are plotted as a function of $\boldsymbol{q}$ and ϵ in Figs. 3 (a,b). The Stoner continuum thus obtained have a finite weight only above some critical energy, $\epsilon \geq \omega_c$. This feature is because the energy dispersions of the fermionic excitations, say $\pm\Delta_k$, are fully gapped in the Z_2 planar state;

$$\Delta_k = \frac{1}{4}J_1^2 D^2(s_x^2+s_y^2) + J_2^2\chi^2 c_x^2 c_y^2 + J_2^2\eta^2 s_x^2 s_y^2 > 0. \tag{36}$$

One should also notice that continuum in $\mathrm{Im}\chi_{zz}(\boldsymbol{q}, \epsilon)$ has no spectral weight at $\boldsymbol{q} = (\pi, \pi)$, because of the staggered $U(1)$ spin-rotational symmetry, Eq. (18).

To capture the low-energy collective excitations, which emerge below these continuum spectra, we next include the effect of fluctuations of the auxiliary fields and the gauge fields around their saddle point values. The fluctuation fields for the Z_2 planar state are given by the following 35 elements:

$$\begin{aligned}
&\boldsymbol{r}(\boldsymbol{j},\tau)\\
&\equiv\big[\mathrm{Re}E_{x,3},\ \mathrm{Im}E_{x,3},\ \mathrm{Re}E_{y,3},\ \mathrm{Im}E_{y,3},\\
&\quad \mathrm{Re}D_{x,3},\ \mathrm{Im}D_{x,3},\ \mathrm{Re}D_{y,3},\ \mathrm{Im}D_{y,3},\\
&\quad \mathrm{Re}E_{x,1},\ \mathrm{Im}E_{x,1},\ \mathrm{Re}E_{y,1},\ \mathrm{Im}E_{y,1},\\
&\quad \mathrm{Re}D_{x,1}-D,\ \mathrm{Im}D_{x,1},\ \mathrm{Re}D_{y,1},\ \mathrm{Im}D_{y,1},\\
&\quad \mathrm{Re}E_{x,2},\ \mathrm{Im}E_{x,2},\ \mathrm{Re}E_{y,2},\ \mathrm{Im}E_{y,2},\\
&\quad \mathrm{Re}D_{x,2},\ \mathrm{Im}D_{x,2},\ \mathrm{Re}D_{y,2}-D,\ \mathrm{Im}D_{y,2},\\
&\quad \mathrm{Re}\chi_{x+y}-\chi,\ \mathrm{Re}\chi_{x-y}-\chi,\ \mathrm{Re}\eta_{x+y}-\eta,\ \mathrm{Re}\eta_{x-y}+\eta,\\
&\quad \mathrm{Im}\chi_{x+y},\ \mathrm{Im}\chi_{x-y},\ \mathrm{Im}\eta_{x+y},\mathrm{Im}\eta_{x-y},\ ia^1_\tau,\ ia^2_\tau,\ ia^3_\tau\big].
\end{aligned}\tag{37}$$

Here, $D_{\nu,\mu}$ and $E_{\nu,\mu}$ with $\nu = x, y$ stand for the μ-th component of the d-vector in the Cooper channel and the excitonic channel, respectively, both of which are defined on the nearest neighbor ferromagnetic links as

$$\begin{aligned}
D_{\nu,\mu}\Big(\boldsymbol{j}+\frac{\boldsymbol{e}_\nu}{2},\tau\Big) &\equiv i\big\langle f_{\boldsymbol{j},\alpha}\big[\sigma_2\sigma_\mu\big]_{\alpha\beta}f_{\boldsymbol{j}+\boldsymbol{e}_\nu,\beta}\big\rangle,\\
E_{\nu,\mu}\Big(\boldsymbol{j}+\frac{\boldsymbol{e}_\nu}{2},\tau\Big) &\equiv \big\langle f^\dagger_{\boldsymbol{j},\alpha}\big[\sigma_\mu\big]_{\alpha\beta}f_{\boldsymbol{j}+\boldsymbol{e}_\nu,\beta}\big\rangle,
\end{aligned}$$

whereas $\chi_{x\pm y}/\eta_{x\pm y}$ denotes the singlet Cooper/excitonic pairing defined on the $x \pm y$-links as

$$\begin{aligned}
\eta_{x\pm y}\Big(\boldsymbol{j}+\frac{\boldsymbol{e}_x\pm\boldsymbol{e}_y}{2},\tau\Big) &\equiv -i\big\langle f_{\boldsymbol{j},\alpha}\big[\sigma_2\big]_{\alpha\beta}f_{\boldsymbol{j}+\boldsymbol{e}_x\pm\boldsymbol{e}_y,\beta}\big\rangle,\\
\chi_{x\pm y}\Big(\boldsymbol{j}+\frac{\boldsymbol{e}_x\pm\boldsymbol{e}_y}{2},\tau\Big) &\equiv \big\langle f^\dagger_{\boldsymbol{j},\alpha}f_{\boldsymbol{j}+\boldsymbol{e}_x\pm\boldsymbol{e}_y,\alpha}\big\rangle.
\end{aligned}$$

In terms of these fluctuation fields, the single-particle Green function appearing in Eq. (9) takes the form

$$\begin{aligned}
&\boldsymbol{G}^{-1}_{(\boldsymbol{k},n,a|\boldsymbol{k}',n',a)} = \boldsymbol{G}^{-1}_{0,(\boldsymbol{k},n,a|\boldsymbol{k}',n',a)}\\
&+\frac{1}{\sqrt{\beta N_\Lambda}}\sum_{\boldsymbol{q}}\sum_m \delta_{\boldsymbol{k},\boldsymbol{k}'+\boldsymbol{q}}\delta_{n,n'+m}r_\alpha(\boldsymbol{q},m)\boldsymbol{v}_\alpha(\boldsymbol{k},\boldsymbol{k}'),
\end{aligned}\tag{38}$$

where the bosonic fluctuation fields $\boldsymbol{r}$ are transformed as

$$r_\alpha(\boldsymbol{q},m) \equiv \frac{1}{\sqrt{\beta N_\Lambda}}\sum_{\boldsymbol{j}}\int_0^\beta d\tau\, e^{-i\boldsymbol{j}\cdot\boldsymbol{q}-i\epsilon_m\tau}r_\alpha(\boldsymbol{j},\tau).$$

The index α specifies the type of the fluctuation fields ($\alpha = 1, \cdots, 35$). The summation over the repeated index α is made implicit and will be so henceforth. In the same sequence as in Eq. (37), the internal vertices $\boldsymbol{v}_\alpha$ are explicitly given by the 4×4 matrix forms

$$\begin{aligned}
&\boldsymbol{v}(\boldsymbol{k},\boldsymbol{k}')\\
&\equiv\big[-\overline{c}_x\boldsymbol{\gamma}_{35},\ -\overline{s}_x\boldsymbol{\gamma}_{12},\ -\overline{c}_y\boldsymbol{\gamma}_{35},\ -\overline{s}_y\boldsymbol{\gamma}_{12},\\
&\quad \overline{s}_x\boldsymbol{\gamma}_1,\ \overline{s}_x\boldsymbol{\gamma}_{14},\ \overline{s}_y\boldsymbol{\gamma}_1,\ \overline{s}_y\boldsymbol{\gamma}_{14},\\
&\quad -\overline{c}_x\boldsymbol{\gamma}_{15},\ -\overline{s}_x\boldsymbol{\gamma}_{23},\ -\overline{c}_y\boldsymbol{\gamma}_{15},\ -\overline{s}_y\boldsymbol{\gamma}_{23},\\
&\quad -\overline{s}_x\boldsymbol{\gamma}_3,\ -\overline{s}_x\boldsymbol{\gamma}_{34},\ -\overline{s}_y\boldsymbol{\gamma}_3,\ -\overline{s}_y\boldsymbol{\gamma}_{34},\\
&\quad \overline{c}_x\boldsymbol{\gamma}_{31},\ \overline{s}_x\boldsymbol{\gamma}_{25},\ \overline{c}_y\boldsymbol{\gamma}_{31},\ \overline{s}_y\boldsymbol{\gamma}_{25},\\
&\quad \overline{s}_x\boldsymbol{\gamma}_5,\ -\overline{s}_x\boldsymbol{\gamma}_{45},\ \overline{s}_y\boldsymbol{\gamma}_5,\ -\overline{s}_y\boldsymbol{\gamma}_{45},\\
&\quad -\overline{c}'_{x+y}\boldsymbol{\gamma}_4,\ -\overline{c}'_{x-y}\boldsymbol{\gamma}_4,\ \overline{c}'_{x+y}\boldsymbol{\gamma}_2,\ \overline{c}'_{x-y}\boldsymbol{\gamma}_2,\\
&\quad -\overline{s}'_{x+y}\boldsymbol{\gamma}_0,\ -\overline{s}'_{x-y}\boldsymbol{\gamma}_0,\ \overline{c}'_{x+y}\boldsymbol{\gamma}_{24},\ \overline{c}'_{x-y}\boldsymbol{\gamma}_{24},\ -\boldsymbol{\gamma}_2,\ \boldsymbol{\gamma}_{24},\ \boldsymbol{\gamma}_4\big],
\end{aligned}\tag{39}$$

where

$$\begin{aligned}
\overline{c}_\mu &= \frac{J_1}{2}\cos\Big(\frac{k_\mu+k'_\mu}{2}\Big),\\
\overline{s}_\mu &= \frac{J_1}{2}\sin\Big(\frac{k_\mu+k'_\mu}{2}\Big),\\
\overline{c}'_{x\pm y} &= \frac{J_2}{2}\cos\Big(\frac{k_x+k'_x\pm k_y\pm k'_y}{2}\Big),\\
\overline{s}'_{x\pm y} &= \frac{J_2}{2}\sin\Big(\frac{k_x+k'_x\pm k_y\pm k'_y}{2}\Big).
\end{aligned}$$

To obtain the quantum corrections to the Hartree-Fock contribution [Eqs. (33) or (35)], we expand the action in term of the fluctuation fields $\boldsymbol{r}$;

$$\begin{aligned}\mathcal{S} =&\mathcal{S}_{\rm I} - \frac{1}{2N}\sum_{a=1}^{N}{\rm Tr}\ln\left[\boldsymbol{G}^{-1}\right]\\ =&\mathcal{S}^{(0)} + \mathcal{S}^{(1)}_{\alpha} r_{\alpha} + \mathcal{S}^{(2)}_{\alpha,\alpha'} r_{\alpha} r_{\alpha'}\\ &+\sum_{n=3}^{\infty} S^{(n)}_{\alpha_1,\alpha_2,\cdots,\alpha_n} r_{\alpha_1} r_{\alpha_2}\cdots r_{\alpha_n}. \end{aligned} \tag{40}$$

The coefficients in Eq. (40) are given in terms of the internal vertex $\boldsymbol{v}_{\alpha}$ as

$$\begin{aligned}\mathcal{S}^{(n)}_{\alpha_1,\alpha_2,\cdots,\alpha_n} =& \frac{\partial \mathcal{S}_{\rm I}}{\partial r_{\alpha_1}}\delta_{n,1} + \frac{1}{2}\frac{\partial^2 \mathcal{S}_{\rm I}}{\partial r_{\alpha_1}\partial r_{\alpha_2}}\delta_{n,2}\\ &+\frac{(-1)^n}{2Nn(\beta N_{\Lambda})^{n/2}}\sum_{a=1}^{N}{\rm Tr}\big[\boldsymbol{G}_0\boldsymbol{v}_{\alpha_1}\boldsymbol{G}_0\boldsymbol{v}_{\alpha_2}\cdots\boldsymbol{G}_0\boldsymbol{v}_{\alpha_n}\big] \end{aligned} \tag{41}$$

with $n \geq 1$. The trace here is taken over the momentum, Matsubara frequency, spin, and particle-hole indices.

To calculate the correlation functions Eqs. (30) and (31), we expand the action in the small field h^{aa} with a certain flavor a in the form

$$\begin{aligned}\mathcal{S} =& \overline{\mathcal{S}}^{(0)} + \overline{\mathcal{S}}^{(2)}_{\alpha,\alpha'} r_{\alpha} r_{\alpha'} + \sum_{n=3}^{\infty}\overline{\mathcal{S}}^{(n)}_{\alpha_1,\alpha_2,\cdots,\alpha_n} r_{\alpha_1} r_{\alpha_2}\cdots r_{\alpha_n}\\ &+\frac{1}{N}\sum_{\mu=1}^{3}\sum_{n=1}^{\infty}\overline{\mathcal{S}}^{(1,n)}_{\mu;\alpha_1,\cdots,\alpha_n} r_{\alpha_1}\cdots r_{\alpha_n} h^{aa}_{\mu}\\ &+\frac{1}{N}\sum_{\mu,\nu=1}^{3}\sum_{n=0}^{\infty}\overline{\mathcal{S}}^{(2,n)}_{\mu,\nu;\alpha_1,\cdots,\alpha_n} r_{\alpha_1}\cdots r_{\alpha_n} h^{aa}_{\mu} h^{aa}_{\nu}, \end{aligned} \tag{42}$$

where the overline stands for its evaluation at the zero field, e.g., $\overline{\mathcal{S}}^{(0)} = \mathcal{S}^{(0)}|_{h=0}$ and $\overline{\mathcal{S}}^{(2)}_{\alpha,\alpha'} = \mathcal{S}^{(2)}_{\alpha,\alpha'}|_{h=0}$. By definition, the expansion around the saddle point has no linear term in $\boldsymbol{r}$. The coefficients $\overline{\mathcal{S}}^{(1,n)}$ and $\overline{\mathcal{S}}^{(2,n)}$ are given by

$$\overline{\mathcal{S}}^{(1,n)}_{\mu;\alpha_1,\cdots,\alpha_n} \equiv N\frac{\partial \mathcal{S}^{(n)}_{\alpha_1,\cdots,\alpha_n}}{\partial h^{aa}_{\mu}}\Big|_{h=0}, \tag{43}$$

$$\overline{\mathcal{S}}^{(2,n)}_{\mu,\nu;\alpha_1,\cdots,\alpha_n} \equiv \frac{N}{2}\frac{\partial^2 \mathcal{S}^{(n)}_{\alpha_1,\cdots,\alpha_n}}{\partial h^{aa}_{\mu}\partial h^{aa}_{\nu}}\Big|_{h=0} \tag{44}$$

with $n \geq 0$. In Eq. (42), we have also used the relation $\overline{S}^{(1,0)}_{\mu;} \sim \sum_{k,n}{\rm Tr}[g_0(k,i\omega_n)\boldsymbol{u}_{\mu}] = 0$, which already appeared in the second term of Eq. (34). The Hartree-Fock susceptibility $\chi^{aa,(0)}_{\mu\nu}$ corresponds to $\overline{S}^{(2,0)}_{\mu,\nu;}$.

The bilinear term in $\boldsymbol{r}$ is given by

$$\overline{\mathcal{S}}^{(2)}_{\alpha,\alpha'} = \frac{1}{2}\frac{\partial^2 \mathcal{S}_{\rm I}}{\partial r_{\alpha}\partial r_{\alpha'}} + \frac{1}{4\beta N_{\Lambda}}\sum_{k,n}{\rm Tr}\big[\boldsymbol{g}_0\,\boldsymbol{v}_{\alpha}\,\boldsymbol{g}_0\,\boldsymbol{v}_{\alpha'}\big]. \tag{45}$$

Other $\overline{\mathcal{S}}^{(n)}$ (with $n > 2$), $\overline{\mathcal{S}}^{(1,n)}$, and $\overline{\mathcal{S}}^{(2,n)}$ contain one loop composed by multiple one-particle green functions. For example, $\overline{\mathcal{S}}^{(1,1)}$, and $\overline{\mathcal{S}}^{(2,1)}$ take the following forms

$$\overline{\mathcal{S}}^{(1,1)}_{\mu;\alpha} = \frac{1}{4\beta N_{\Lambda}}\sum_{k,n}{\rm Tr}[\boldsymbol{g}_0\boldsymbol{u}_{\mu}\boldsymbol{g}_0\boldsymbol{v}_{\alpha}], \tag{46}$$

$$\begin{aligned}\overline{\mathcal{S}}^{(2,1)}_{\mu,\nu;\alpha} =& -\frac{1}{16(\beta N_{\Lambda})^{3/2}}\sum_{k,n}\Big\{{\rm Tr}[\boldsymbol{g}_0\boldsymbol{u}_{\nu}\boldsymbol{g}_0\boldsymbol{u}_{\mu}\boldsymbol{g}_0\boldsymbol{v}_{\alpha}]\\ &+{\rm Tr}[\boldsymbol{g}_0\boldsymbol{u}_{\mu}\boldsymbol{g}_0\boldsymbol{u}_{\nu}\boldsymbol{g}_0\boldsymbol{v}_{\alpha}]\Big\}, \end{aligned} \tag{47}$$

where $\boldsymbol{k}$ and $i\omega_n$ denote the momentum and the frequency inside of the loop. The trace in Eqs. (45-47) is only over the particle-hole and spin index. Observing these expressions, notice that $\overline{\mathcal{S}}^{(1,n)}_{\mu;\alpha_1,\cdots,\alpha_n}$ and $\overline{\mathcal{S}}^{(2;n)}_{\mu,\nu;\alpha_1,\cdots,\alpha_n}$ as well as $\overline{\mathcal{S}}^{(n)}_{\alpha_1,\cdots,\alpha_n}$ are generally functions of order unity in the large-N limit.

Based on Eq. (42), spin-spin correlation functions $\chi^{aa}_{\mu\nu} \equiv \chi^{aa}_{\mu\nu,{\rm I}} + \chi^{aa}_{\mu\nu,{\rm II}}$ can be expanded as[15]

$$\chi^{aa}_{\mu\nu,{\rm I}}(\boldsymbol{q},i\epsilon_n) = -\frac{1}{Z}\int d\boldsymbol{r}\left(\sum_{n=0}^{\infty}\overline{\mathcal{S}}^{(2,n)}_{\mu,\nu;\alpha_1,\cdots,\alpha_n} r_{\alpha_1}\cdots r_{\alpha_n}\right)\sum_{m=0}^{\infty}\frac{(-N)^m}{m!}\Big(\sum_{l=3}^{\infty}\overline{\mathcal{S}}^{(l)}_{\alpha_1,\cdots,\alpha_l} r_{\alpha_1}\cdots r_{\alpha_l}\Big)^m e^{-N\overline{\mathcal{S}}^{(2)}_{\alpha,\alpha'} r_{\alpha} r_{\alpha'}}, \tag{48}$$

$$\begin{aligned}\chi^{aa}_{\mu\nu,{\rm II}}(\boldsymbol{q},i\epsilon_n) =& \frac{1}{Z}\int d\boldsymbol{r}\left(\sum_{n=1}^{\infty}\overline{\mathcal{S}}^{(1,n)}_{\mu;\alpha_1,\cdots,\alpha_n} r_{\alpha_1}\cdots r_{\alpha_n}\right)\Big(\sum_{l=1}^{\infty}\overline{\mathcal{S}}^{(1,l)}_{\nu;\alpha_1,\cdots,\alpha_l} r_{\alpha_1}\cdots r_{\alpha_l}\Big)\\ &\times\sum_{m=0}^{\infty}\frac{(-N)^m}{m!}\Big(\sum_{j=3}^{\infty}\overline{\mathcal{S}}^{(j)}_{\alpha_1,\cdots,\alpha_j} r_{\alpha_1}\cdots r_{\alpha_j}\Big)^m e^{-N\overline{\mathcal{S}}^{(2)}_{\alpha,\alpha'} r_{\alpha} r_{\alpha'}}, \end{aligned} \tag{49}$$

where $\overline{\mathcal{S}}_0$ was omitted for simplicity. The Gaussian integrals over the real-valued fields $\boldsymbol{r}$ can be taken, reducing even numbers of the fields to a sum over all the possible pairwise contractions among the fields;

$$\int d\boldsymbol{r}\, r_1\cdots r_{2k}\,\exp\big[-N\overline{\mathcal{S}}^{(2)}_{\alpha,\alpha'} r_{\alpha} r_{\alpha'}\big] = \sum_{\sigma}\frac{1}{N^k}[\overline{\mathcal{S}}^{(2),-1}]_{\sigma(1),\sigma(2)}[\overline{\mathcal{S}}^{(2),-1}]_{\sigma(3),\sigma(4)}\cdots[\overline{\mathcal{S}}^{(2),-1}]_{\sigma(2k-1),\sigma(2k)}. \tag{50}$$

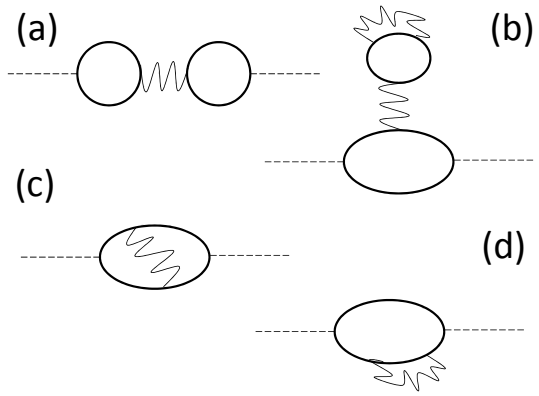

FIG. 4: $1/N$-contributions to correlation functions, where a dotted line denotes external fields, a wavy line is the RPA propagator and a solid line is single-particle Green function. (a) contributes to $\chi^{aa}_{\mu\mu,\mathrm{II}}(q,i\epsilon_n)$, while (b,c,d) to $\chi^{aa}_{\mu\mu,\mathrm{I}}(q,i\epsilon_n)$. (a) spin-wave term, (b,d) Hartree-Fock (HF) term with renormalized single-particle Green functions. (c) HF term with the vertex correction.

The summation over σ runs over the arbitrary permutations among the $2k$ indices.

To enumerate all the contractions possible in Eqs. (48-49), use Feynman diagrams as depicted in Fig. 4. In these diagrams, all coefficients $\overline{S}^{(n)}$ (with $n \geq 3$), $\overline{S}^{(1,n)}$, and $\overline{S}^{(2,n)}$ in Eq. (42) contain single loops made by solid lines and vertices. Each solid line denotes a single-particle Green function, and two neighboring solid lines are always mediated by either an external vertex $\boldsymbol{u}_\alpha$ or an internal vertex $\boldsymbol{v}_\alpha$. From the external vertex, a dotted line representing an external field is emitted. Any internal vertex is connected with one and only one of others internal vertices by a wavy line representing the 'RPA propagator', $[\overline{\mathcal{S}}^{(2),-1}]_{\alpha,\beta}$.

In the large-N limit, each single closed loop appearing in $\overline{S}^{(n)}$ (with $n \geq 3$) is in the order of unity due to the flavor degree of freedom and the prefactor $1/N$. Each loop connected to any external field (dotted line) appearing in $\overline{S}^{(1,n)}$ or $\overline{S}^{(2,n)}$ is also in the order of unity as the flavor index of the internal line is set to 'a'. From Eq. (50), a RPA propagator is accompanied by factor N^{-1}. This concludes that the leading contribution to the spin-spin correlation function in the large-N limit is its saddle-point estimation, Eq. (35) [see Fig. 3(d)] and the first order quantum corrections in the order of $1/N$ are given by the Feynman diagrams depicted in Fig. 4. Those diagrams which vanish by themselves have been already omitted.

Notice first that Figs. 4(b–d) take the same structure as that of the mean-field diagram depicted in Fig. 3(d), where the difference can be solely attributed to a proper renormalization of the single-particle Green function (b,d) or that of the external vertices (c). Thus, their major contribution is more or less modification of shape and intensity of the Stoner continuum. In Fig. 4(a), on the other hand, the momentum and energy carried by one of the external lines are transmitted to the other only through the RPA propagator, into which various collective excitations including magnetic Goldstone modes are encoded. Thus, some of low-energy poles of the RPA propagator generally show up as coherent bosonic peaks in the imaginary part of Fig. 4(a).

To see this situation explicitly, we henceforth derive the expression for Fig. 4(a). Notice first that a 4×4 BdG Hamiltonian for the Z_2 planar state satisfies the following symmetry relations

$$\boldsymbol{\gamma}_3 \boldsymbol{H}^{(0)}_{k_x,k_y} \boldsymbol{\gamma}_3 = \boldsymbol{H}^{(0)}_{k_x,k_y+\pi}, \quad \boldsymbol{\gamma}_5 \boldsymbol{H}^{(0)}_{k_x,k_y} \boldsymbol{\gamma}_5 = \boldsymbol{H}^{(0)}_{k_x+\pi,k_y}. \tag{51}$$

These symmetries require that the RPA propagator defined in Eq. (45) is always a block diagonal matrix with respect to the following four groups of fluctuation fields:

$$\boldsymbol{R}_1 \equiv \mathrm{Re}D_{y,3}\, \boldsymbol{e}^1_1 + \mathrm{Im}D_{x,3}\, \boldsymbol{e}^1_2 + \mathrm{Im}E_{x,3}\, \boldsymbol{e}^1_3 + \mathrm{Re}E_{y,3}\, \boldsymbol{e}^1_4, \tag{52}$$

$$\boldsymbol{R}_2 \equiv \mathrm{Re}D_{x,3}\, \boldsymbol{e}^2_1 + \mathrm{Im}D_{y,3}\, \boldsymbol{e}^2_2 + \mathrm{Im}E_{y,3}\, \boldsymbol{e}^2_3 + \mathrm{Re}E_{x,3}\, \boldsymbol{e}^2_4, \tag{53}$$

$$\begin{aligned}\boldsymbol{R}_3 \equiv & \mathrm{Re}D_{x,2}\, \boldsymbol{e}^3_1 + \mathrm{Re}D_{y,1}\, \boldsymbol{e}^3_2 + \mathrm{Im}D_{y,2}\, \boldsymbol{e}^3_3 \\ & + \mathrm{Im}D_{x,1}\, \boldsymbol{e}^3_4 + \mathrm{Im}E_{y,2}\, \boldsymbol{e}^3_5 + \mathrm{Im}E_{x,1}\, \boldsymbol{e}^3_6 \\ & + \mathrm{Re}E_{x,2}\, \boldsymbol{e}^3_7 + \mathrm{Re}E_{y,1}\, \boldsymbol{e}^3_8 + \mathrm{Im}\chi_{x+y}\, \boldsymbol{e}^3_9 \\ & + \mathrm{Im}\chi_{x-y}\, \boldsymbol{e}^3_{10} + \mathrm{Im}\eta_{x+y}\, \boldsymbol{e}^3_{11} + \mathrm{Im}\eta_{x-y}\, \boldsymbol{e}^3_{12} \\ & + i a^3_\tau\, \boldsymbol{e}^3_{13} + i a^1_\tau\, \boldsymbol{e}^3_{14},\end{aligned} \tag{54}$$

$$\begin{aligned}\boldsymbol{R}_4 \equiv & \big(\mathrm{Re}D_{x,1} - D\big)\, \boldsymbol{e}^4_1 + \big(\mathrm{Re}D_{y,2} - D\big)\, \boldsymbol{e}^4_2 \\ & + \mathrm{Im}D_{y,1}\, \boldsymbol{e}^4_3 + \mathrm{Im}D_{x,2}\, \boldsymbol{e}^4_4 + \mathrm{Im}E_{y,1}\, \boldsymbol{e}^4_5 \\ & + \mathrm{Im}E_{x,2}\, \boldsymbol{e}^4_6 + \mathrm{Re}E_{x,1}\, \boldsymbol{e}^4_7 + \mathrm{Re}E_{y,2}\, \boldsymbol{e}^4_8 \\ & + \big(\mathrm{Re}\chi_{x+y} - \chi\big)\, \boldsymbol{e}^4_9 + \big(\mathrm{Re}\chi_{x-y} - \chi\big)\, \boldsymbol{e}^4_{10} \\ & + \big(\mathrm{Re}\eta_{x+y} - \eta\big)\, \boldsymbol{e}^4_{11} + \big(\mathrm{Re}\eta_{x-y} + \eta\big)\, \boldsymbol{e}^4_{12} \\ & + i a^2_\tau\, \boldsymbol{e}^4_{13},\end{aligned} \tag{55}$$

where $\{\boldsymbol{e}^\mu_\alpha\}$ denotes the orthonormal basis of 35-dimensional space $\mathbb{R}^{35}$ and the renamed fluctuation fields $\{R_{\mu,\alpha}\}$ are defined through $\boldsymbol{R}_\mu = R_{\mu,\alpha}\boldsymbol{e}^\mu_\alpha$. Using this representation, the Gaussian part of the action is indeed decomposed into four parts,

$$[\overline{\mathcal{S}}^{(2)}]_{\alpha,\beta} r_\alpha r_\beta = \sum_{\mu=1}^{4} [\overline{\mathcal{S}}^{(2)}_{\mu\mu}]_{\alpha,\beta} R_{\mu,\alpha} R_{\mu,\beta}, \tag{56}$$

where the matrix elements inside of each block are given as

$$\begin{aligned}\big[\overline{\mathcal{S}}^{(2)}_{\mu\mu}(\boldsymbol{q}, i\epsilon_n)\big]_{\alpha,\beta} \equiv & \frac{1}{2}\frac{\partial^2 \mathcal{S}_{\mathrm{I}}}{\partial r_{\mu,\alpha}\partial r_{\mu,\beta}} + \frac{1}{4\beta N_\Lambda}\sum_{\boldsymbol{k},n} \\ & \times \mathrm{Tr}\big[\boldsymbol{g}_0(\boldsymbol{k}+\boldsymbol{q}, i\omega_n + i\epsilon_n)\boldsymbol{v}_{\mu,\beta}\, \boldsymbol{g}_0(\boldsymbol{k}, i\omega_n)\boldsymbol{v}_{\mu,\alpha}\big]\end{aligned} \tag{57}$$

in the momentum representation. The internal vertices here are also renamed such that $\sum_\alpha r_\alpha \boldsymbol{v}_\alpha = \sum_{\mu=1}^4 \sum_\alpha R_{\mu,\alpha}\boldsymbol{v}_{\mu,\alpha}$.

One can also see that, under Eq. (51), any fluctuation fields in Eq. (55) are disconnected from the external magnetic fields, while those in Eqs. (52)–(54) are coupled with the external vertices in the form

$$\overline{\mathcal{S}}^{(1,1)}_{\mu;\alpha}\, h_\mu r_\alpha = \sum_{\mu=1}^{3} \big[\overline{\mathcal{S}}^{(1,1)}_{\mu;\mu}\big]_\alpha h_\mu R_{\mu,\alpha}, \tag{58}$$

where

$$\big[\overline{\mathcal{S}}^{(1,1)}_{\mu;\mu}(\boldsymbol{q}, i\epsilon_n)\big]_\alpha \equiv \frac{1}{4\beta N_\Lambda}\sum_{\boldsymbol{k},n} \times \mathrm{Tr}\big[\boldsymbol{g}_0(\boldsymbol{k}+\boldsymbol{q}, i\omega_n + i\epsilon_n)\boldsymbol{u}_\mu\, \boldsymbol{g}_0(\boldsymbol{k}, i\omega_n)\boldsymbol{v}_{\mu,\alpha}\big]. \tag{59}$$

Using Eqs. (57) and (59), we finally obtain the contribution from Fig. 4(a) as

$$\chi^{(1)}_{\mu\mu,\mathrm{II}}(\boldsymbol{q}, i\epsilon_n) = \big[\overline{\mathcal{S}}^{(1,1)}_{\mu;\mu}\big]_\alpha \big[\overline{\mathcal{S}}^{(2),-1}_{\mu\mu}\big]_{\alpha,\beta} \big[\overline{\mathcal{S}}^{(1,1)}_{\mu;\mu}\big]_\beta. \tag{60}$$

Among this equation, $\overline{\mathcal{S}}^{(1,1)}_{\mu;\mu}$ clearly has no finite imaginary part, provided that $|\mathrm{Re}z| < \min_{\boldsymbol{k}}(\Delta_{\boldsymbol{k}+\boldsymbol{q}}+\Delta_{\boldsymbol{k}})$, since Eq. (59) has the same structure as the Hartree-Fock solution Eq. (35). Namely, for any μ and α, it always has the form

$$\big[\overline{\mathcal{S}}^{(1,1)}_{\mu;\mu}(\boldsymbol{q}, z)\big]_\alpha = \sum_{\boldsymbol{k}} \frac{A_{\boldsymbol{k},\boldsymbol{q},\alpha}(z)}{-z^2 + (\Delta_{\boldsymbol{k}+\boldsymbol{q}} + \Delta_{\boldsymbol{k}})^2}, \tag{61}$$

where the numerator is a regular function of z and real-valued on the real-axis of z. As such, any finite contribution to $\mathrm{Im}\chi^{(1)}_{\mu\mu,\mathrm{II}}(\boldsymbol{q},\epsilon)$ below the Stoner continuum, $\epsilon < \min_{\boldsymbol{k}}(\Delta_{\boldsymbol{k}+\boldsymbol{q}} + \Delta_{\boldsymbol{k}})$, can be solely attributed to the pole contributions in the RPA propagator, i.e., the zeros of the eigenvalues of Eq. (57).

IV. DYNAMICAL SPIN STRUCTURE FACTORS

In this section, we discuss the dynamical spin structure obtained from the large-N expansion up to the first order of N^{-1}. The spectra of $\mathrm{Im}\chi^{(1)}_{zz,\mathrm{II}}(\boldsymbol{q},\epsilon)$ and $\mathrm{Im}\chi^{(1)}_{+-,\mathrm{II}}(\boldsymbol{q},\epsilon)$ at the zero temperature are calculated numerically based on Eqs. (57)–(61). Their typical plots are shown in Figs. 5 and 6 for the parameter point $J_2/J_1 = 1.1$, which is inside the Z_2 planar phase, i.e., $J_{c,1} > 1.1 > J_{c,2}$ (see Fig. 2). For simplicity, the fluctuations of the temporal gauge fields, ia^μ_τ ($\mu = 1, 2, 3$), are not included in these calculations, so that only the pairing fields comprise these collective excitations.

In the next two subsections (Secs. IV A and IV B), we first describe the character of these low energy collective modes, especially focusing on gapless modes at the momentum points $\boldsymbol{q} = (0, 0)$ and $\boldsymbol{q} = (\pi, 0)$. When the relative ratio between FM J_1 and AF J_2 is changed to $J_2/J_1 = J_{c,2}$, the boundary to the neighboring U(1) planar phase, two of the gapped bosonic modes at the (π, π) momentum point become gapless (see Fig. 7), which correspond to the appearance of gapless gauge excitations ('photon-like' excitation) in the $U(1)$ planar state. In Sec. IV C, we will argue that, in the $U(1)$ planar phase, the mass of two *other* gapped magnetic modes at the (π, π) momentum point simultaneously vanishes, leading to a breakdown of certain symmetries possessed by the Z_2 planar state (see Fig. 8). These symmetry breakings are actually consistent with the 'confinement effect' postulated in this $U(1)$ planar state.

A. Near Γ-point

The Z_2 planar state breaks all the spin-rotational symmetries, while preserves the translational symmetries of the square lattice. Thus, the RPA propagator generally has three spin wave modes which are gapless only at the Γ-point. The corresponding fluctuation fields take the following forms at $\boldsymbol{q} = (0, 0)$:

$$\phi_1 \equiv \frac{1}{\sqrt{2}}\big(\boldsymbol{e}^3_1 - \boldsymbol{e}^3_2\big), \quad \phi_2 \equiv \boldsymbol{e}^1_1, \quad \phi_3 \equiv \boldsymbol{e}^2_1. \tag{62}$$

The ϕ_1-mode and $\phi_{2,3}$-modes appear, respectively, as the gapless excitations in the longitudinal and transverse dynamical spin structure factors (see Figs. 5 and 6). Under the mirror reflection which exchanges the x-axis and y-axis, the planar state is symmetric, and the ϕ_2- and ϕ_3-modes are interchanged. Thus, the ϕ_2- and ϕ_3-modes are energetically degenerate along $(0, 0)$ to (π, π), while the degeneracy is lifted along $(0, 0)$ to $(\pi, 0)$ (see Fig. 6).

Near the Γ-point, the spectral weight of these spin wave modes always vanishes as a linear function of the momentum;

$$\mathrm{Im}\chi^{(1)}_{\mu\mu}(\boldsymbol{q},\epsilon) = a|\boldsymbol{q}|\delta(\epsilon - v|\boldsymbol{q}|) + \cdots. \tag{63}$$

This is because the coupling between these spin wave modes and external fields are given by Eq. (61) with the numerator of its right hand side vanishes as a linear function of z and also because eigenvalues of the RPA propagator are always even in the Matsubara frequency. Under the Kramers-Kronig relation, the real part of the static susceptibility acquires a corresponding quantum correction, which does not diverge at $\boldsymbol{q} = 0$. This observation is consistent with the fact that broken spin rotational symmetry is induced by the ordering of the quadrupole moment.

The vanishing spectral weight of the spin-wave modes at the Γ-point was also observed in other class of quadrupole order phases,[17,18] and is a universal feature of spin-nematic states. A similar behavior of the dynamical spin structure factor is also expected in the collinear AF phase, which is stabilized in the strong AF J_2 regime of the present J_1–J_2 model ($J_2 > 0.57J_1$). To distinguish the current Z_2 planar phase from this collinear AF phase, we also need to look into the spin structure factor near the $(\pi, 0)$ or $(0, \pi)$ momentum point (see Sec. IV B).

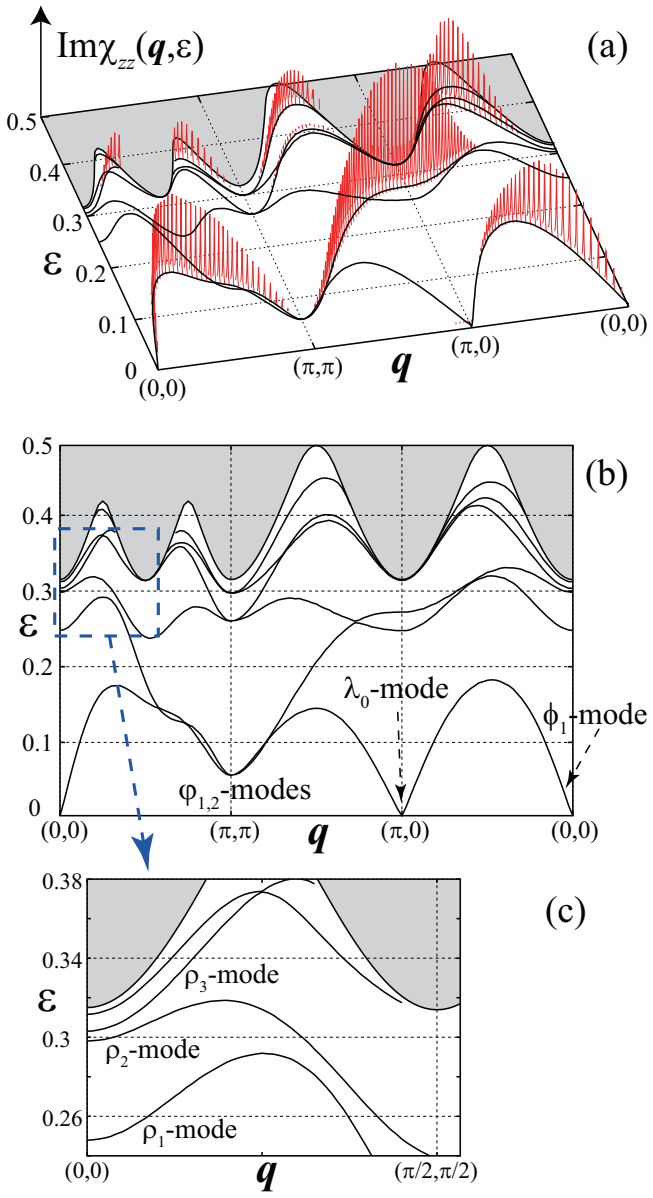

FIG. 5: (Color online) Excitation energy spectrum in the dynamical structure factor $\mathrm{Im}\chi_{zz}(\boldsymbol{q},\epsilon)$ in the Z_2 planar ground state for $J_2/J_1 = 1.1$. The momentum runs along several high symmetric k-points [see Fig. 3(c)]. The grey regions denote Stoner continuum. (a) Spectral wight of the collective modes in $\mathrm{Im}\chi_{zz}(\boldsymbol{q},\epsilon)$. (b) The momentum-energy dispersion relation, showing the collective modes given in the text. (c) The dispersion relation near the Γ-point is enlarged, showing the three gapped squashing modes.

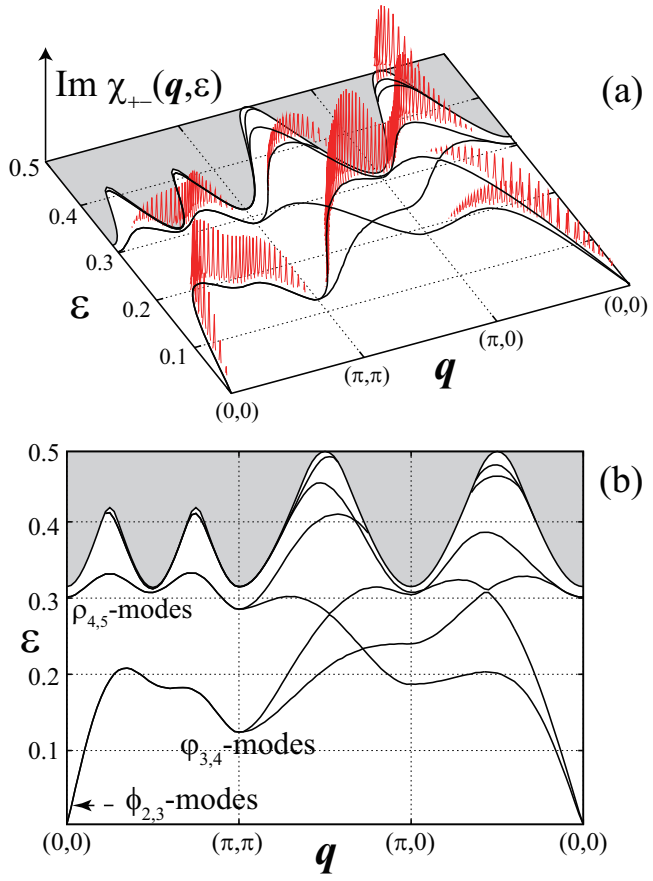

FIG. 6: (Color online) Excitation energy spectrum in the dynamical structure factor $\mathrm{Im}\chi_{+-}(q,\epsilon)$ in the Z_2 planar ground state for $J_2/J_1 = 1.1$. The grey regions denote Stoner continuum. (a) Spectral wight of the collective modes in $\mathrm{Im}\chi_{+-}(\boldsymbol{q},\epsilon)$. (b) The momentum-energy dispersion relations, showing collective modes and gapped squashing modes.

As the Z_2 planar state also breaks the global $SU(2)$ gauge symmetries, one might naively expect that the RPA propagator contains three other gapless modes, which correspond to the Bogoliubov sound modes. However, when their couplings with 'gauge excitations' are included, all of these sound modes will be generally *absorbed* into the gauge fields, only to endow the latter fields with finite Higgs mass:[3,10,19] The Z_2 planar states do not have any *physical* Goldstone modes other than the spin-wave modes.

The low-energy excitations below the Stoner continuum also contain well-defined *massive* modes near the Γ-point [see Figs. 5(b,c) and Fig. 6(b)], which are direct analogue of the so-called squashing modes observed in the superfluid ^{3}He-B phase.[20,21] They take the following form at $\boldsymbol{q} = (0,0)$:

$$\begin{aligned}
&\rho_1 = \alpha_1\big(\boldsymbol{e}_1^3 + \boldsymbol{e}_2^3\big) + \beta_1\big(\boldsymbol{e}_5^3 + \boldsymbol{e}_6^3\big) + \gamma_1\big(\boldsymbol{e}_{11}^3 + \boldsymbol{e}_{12}^3\big),\\
&\rho_2 = \boldsymbol{e}_3^3 - \boldsymbol{e}_4^3, \quad \rho_3 = \alpha_2\big(\boldsymbol{e}_1^3 - \boldsymbol{e}_2^3\big) + \beta_2\big(\boldsymbol{e}_6^3 - \boldsymbol{e}_5^3\big),\\
&\rho_4 = \boldsymbol{e}_4^2, \quad \rho_5 = \boldsymbol{e}_4^1, \quad \cdots . \qquad (64)
\end{aligned}$$

Due to the $SU(2)$ gauge symmetry, these modes are composites not only of the 'squashing' components in the Cooper channel, but also of those in the excitonic channel. Note also that the ρ_3-mode is a linear combination of the spin-wave component and the squashing component in the excitonic channel. This combination becomes possible, because the spin-triplet excitonic pairing operator on the x-link and the spin-triplet Cooper pairing operator

on the y-link do not commute quantum-mechanically in the Z_2 planar state (see Appendix). The spectral weight of all these gapped modes reduce to zero at the Γ-point, while some of them acquire finite weight for finite momentum. In general, however, magnetic properties derived from dynamical spin structure factors cannot be a direct experimental probe for these squashing modes; their weight are quantitatively subdominant.

B. Near $(\pi, 0)$-point and (π, π)-point

When the momentum is away from the Γ-point, all the collective excitations are fully gapped, except for the appearance of two gapless linear modes in $\mathrm{Im}\chi_{zz}(\boldsymbol{q}, \varepsilon)$ at $\boldsymbol{q} = (\pi, 0)$ and $(0, \pi)$ points [see Fig. 5(b)]. The corresponding fluctuation fields are given by $\lambda_0 = \boldsymbol{e}_8^3$ and $\boldsymbol{e}_7^3$, respectively. However, their spectral weight is essentially zero. This is because both fluctuation modes $\boldsymbol{e}_8^3$ and $\boldsymbol{e}_7^3$ do not couple with the external magnetic field at all, $[\overline{\mathcal{S}}_{3;3}^{(1,1)}(\boldsymbol{q}, z)]_8 = [\overline{\mathcal{S}}_{3;3}^{(1,1)}(\boldsymbol{q}, z)]_7 = 0$ at $\boldsymbol{q} \simeq (\pi, 0)$ or $(0, \pi)$. This behavior should be contrasted to the dynamical spin structure expected in the neighboring collinear antiferromagnetic phase, where the spectral weight remains finite even at the gapless points $\boldsymbol{q} = (\pi, 0)$ and $(0, \pi)$, e.g. $\mathrm{Im}\chi_{\mu\mu}((\pi, 0) + \boldsymbol{q}, \epsilon) \simeq b'\delta(\epsilon - u'|\boldsymbol{q}|) + \cdots$ for $|\boldsymbol{q}| \ll 1$ and $\epsilon \ll 1$.

Due to the mirror symmetry with respect to the $(x+y)$-axis, eigenmodes at the (π, π)-point are always doubly degenerate. The lowest gapped excitations comprised of the fluctuation fields

$$\varphi_1 = \alpha \boldsymbol{e}_1^3 + \beta \boldsymbol{e}_3^3 + \gamma \boldsymbol{e}_6^3 + \delta\big(\boldsymbol{e}_9^3 - \boldsymbol{e}_{10}^3\big), \tag{65}$$

$$\varphi_2 = \alpha \boldsymbol{e}_2^3 + \beta \boldsymbol{e}_4^3 + \gamma \boldsymbol{e}_5^3 + \delta\big(\boldsymbol{e}_9^3 + \boldsymbol{e}_{10}^3\big) \tag{66}$$

appear in $\mathrm{Im}\chi_{zz}(\boldsymbol{q}, \epsilon)$. Their momentum-energy dispersion and the spectral weight near the (π, π)-point are shown in Fig. 5. The second lowest gapped modes comprised of the fluctuations

$$\varphi_3 = \epsilon \boldsymbol{e}_1^2 + \zeta \boldsymbol{e}_2^2, \quad \varphi_4 = \epsilon \boldsymbol{e}_1^1 + \zeta \boldsymbol{e}_2^1 \tag{67}$$

appear in $\mathrm{Im}\chi_{+-}(\boldsymbol{q}, \epsilon)$, whose energy dispersion and the spectral weight near the (π, π)-point are shown in Fig. 6. When the momentum approaches this symmetric k-point, the spectral weight of these four gapped modes vanishes as a quadratic function of the momentum, i.e. $\mathrm{Im}\chi_{\mu\mu}((\pi, \pi) + \boldsymbol{q}, \epsilon) \simeq \alpha''|\boldsymbol{q}|^2\delta(\epsilon - m - v''|\boldsymbol{q}|^2)$ for $|\boldsymbol{q}| \ll 1$. The vanishing of the spectral weight at $\boldsymbol{q} = (\pi, \pi)$ is a consequence of the staggered $U(1)$ spin-rotational symmetry in the Z_2 planar state, Eq. (18). As will be described in the next subsection, on decreasing J_2, the φ_1-mode and φ_2-mode become gapless, only to comprise a photon-like dispersion at $J_2/J_1 < J_{c,2}$, where the other two gapped modes [φ_3 and φ_4] simultaneously exhibit instabilities.

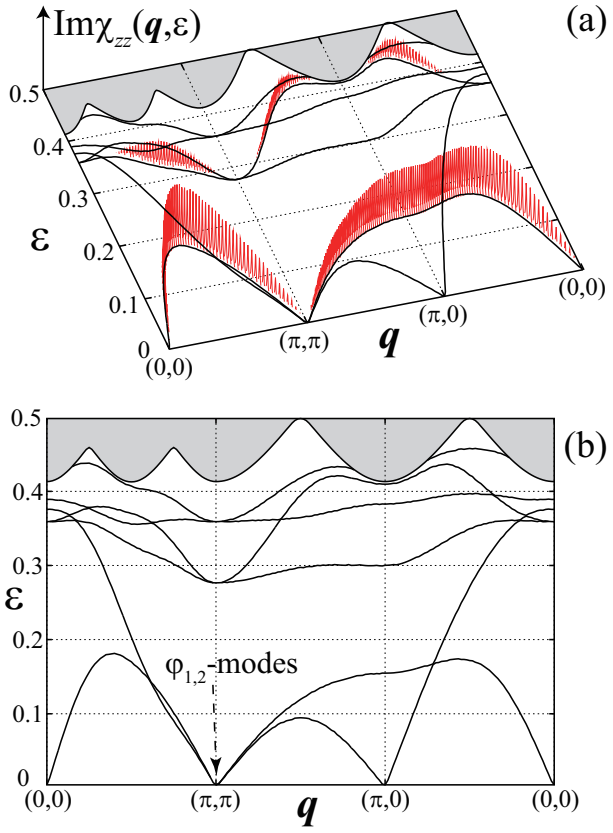

FIG. 7: (Color online) Dynamical structure factor $\mathrm{Im}\chi_{zz}(\boldsymbol{q}, \epsilon)$ at the zero temperature at the critical point between the Z_2 planar and $U(1)$ planar phases, i.e., $J_2/J_1 = J_{c,2} = 1.0448$ (see text). The grey regions denote Stoner continuum. (a) Spectral wight of the collective modes in $\mathrm{Im}\chi_{zz}(\boldsymbol{q}, \epsilon)$. (b) The momentum-energy dispersion relations for the collective modes, showing that the lowest excitations at the (π, π)-point become gapless.

C. Transition to the $U(1)$ planar state and its instability

The saddle point solution suggests that, when the 2nd-neighbor antiferromagnetic exchange J_2 decreases, the d-wave spin-singlet Cooper pairing amplitude η reduces to zero at the critical point $J_2/J_1 = J_{c,2} \simeq 1.0448$, while the spin-triplet Cooper pairing amplitude D and the s-wave excitonic pairing amplitude χ remain finite even beyond the boundary, $J_2/J_1 < J_{c,2}$.[10] Such a planar state in $J_2/J_1 < J_{c,2}$ becomes invariant under the following global $U(1)$ rotation around the 3-axis in the gauge space

$$\Psi_{\boldsymbol{j}}^\dagger \to \Psi_{\boldsymbol{j}}^\dagger e^{i(-1)^{j_x + j_y}\theta\sigma_3}, \quad \Psi_{\boldsymbol{j}} \to e^{-i(-1)^{j_x + j_y}\theta\sigma_3}\Psi_{\boldsymbol{j}} \tag{68}$$

and hence that is dubbed as the $U(1)$ planar state.

Owing to the restoration of this continuous gauge symmetry, some of gapped gauge bosons in the Z_2 planar state become massless at $J_2/J_1 = J_{c,2}$. φ_1-mode and φ_2-modes defined in Eqs. (65,66) are actually spatial components of these gauge bosons, which compose (part of)

a gauge-invariant Maxwell form for $J < J_{c,2}$ (see Fig. 7). Specifically, α and γ in Eqs. (65) and (66) reduce to zero at $J_2/J_1 = J_{c,2}$, where these two modes become

$$\varphi_1^{(c)} = D\, \boldsymbol{e}_3^3 + \chi\, (\boldsymbol{e}_9^3 - \boldsymbol{e}_{10}^3),$$
$$\varphi_2^{(c)} = D\, \boldsymbol{e}_4^3 + \chi\, (\boldsymbol{e}_9^3 + \boldsymbol{e}_{10}^3).$$

Regarding that their amplitudes are infinitesimally small, one can identify these fluctuation fields as the spatial components of the gauge field introduced as

$$\begin{aligned}\mathcal{L} \;=\; \cdots &- \frac{J_1}{4}\sum_{\boldsymbol{j}} \mathrm{Tr}\big[\Psi_{\boldsymbol{j}}^\dagger\, D\sigma_2\, e^{ia_x^3\,\sigma_3}\, \Psi_{\boldsymbol{j}+\boldsymbol{e}_x}\, \sigma_1^T\,\big] \\ &- \frac{J_1}{4}\sum_{\boldsymbol{j}} \mathrm{Tr}\big[\Psi_{\boldsymbol{j}}^\dagger\, D\sigma_2\, e^{ia_y^3\,\sigma_3}\, \Psi_{\boldsymbol{j}+\boldsymbol{e}_y}\, \sigma_2^T\,\big] \\ &- \frac{J_2}{4}\sum_{j} \mathrm{Tr}\big[\Psi_{\boldsymbol{j}}^\dagger\, \chi\sigma_3\, e^{-i(a_x^3+a_y^3)\sigma_3}\, \Psi_{\boldsymbol{j}+\boldsymbol{e}_x+\boldsymbol{e}_y}\big] \\ &- \frac{J_2}{4}\sum_{\boldsymbol{j}} \mathrm{Tr}\big[\Psi_{\boldsymbol{j}}^\dagger\, \chi\sigma_3\, e^{-i(a_x^3-a_y^3)\sigma_3}\, \Psi_{\boldsymbol{j}+\boldsymbol{e}_x-\boldsymbol{e}_y}\big] \qquad (69)\end{aligned}$$

with $a_x^3 = \varphi_2^{(c)}$ and $a_y^3 = \varphi_1^{(c)}$. The $U(1)$ local gauge symmetry implemented by Eq. (68) requires that the spatial component thus introduced, in combination with the staggered component of the temporal gauge field, i.e. $a_0^3 \equiv (-1)^{j_x+j_y}\, a_{\boldsymbol{j},\tau}^3$, must take a gauge invariant quadratic form as their effective action, which turns out to be the Maxwell form[10]

$$F_{\mathrm{gauge}} = \int_0^\beta d\tau \int d^2r \big\{ u\boldsymbol{E}^2 + \frac{K}{2} B^2 \big\}. \qquad (70)$$

The 'emergent' electromagnetic fields are defined as $E_\alpha \equiv \partial_\tau a_x^3 - \partial_\alpha a_0^3$, and $B \equiv \partial_x a_y^3 - \partial_y a_x^3$.

In the $2+1$ dimensional space, this Maxwell form does not suppress the fluctuations of these gauge fields efficiently, so that the $U(1)$ planar state is generally unstable against these fluctuations. That is, the space-time instanton which is allowed by the corresponding compact QED action, $\int_0^\beta \int d^2r \{u\boldsymbol{E}^2 - K\cos(\epsilon_{\alpha\beta}\partial_\alpha a_\beta^3)\}$, proliferate in the $2+1$ dimensional space, only to introduce strong confining potentials between two neutral 'free' fermions (spinon).[22] In the context of spin-singlet quantum spin liquids, it is known that resulting confining phases are accompanied by the reduction of the space group symmetry of original mean-field states.[23]

In the present situation, this symmetry reduction is driven by the condensation of the φ_3-mode and φ_4-mode defined in Eq. (67). Namely, these two modes exhibit instabilities at the same time that the φ_1- and φ_2-modes become massless (see Fig. 8). Since these bosons carry the (π,π)-momentum, their instabilities break the translational symmetries of the square lattice (Fig. 8(c)). Moreover, their condensations also introduce finite z-components of the spin-triplet $\boldsymbol{d}$-vectors connecting nearest neighbor sites (compare Eq. (67) with Eqs. (52,53)), so that they also breaks the staggered $U(1)$ spin-rotational symmetry defined in Eq. (18). Having such 'triplet-dimer' orderings as the background, a pair of spinon and anti-spinon introduced on the uniform condensate is expected to pay those energy cost which are proportional to the spatial distance between these two. Because of this strong confining potential, the pair are spatially confined to each other in the $U(1)$ planar phase.

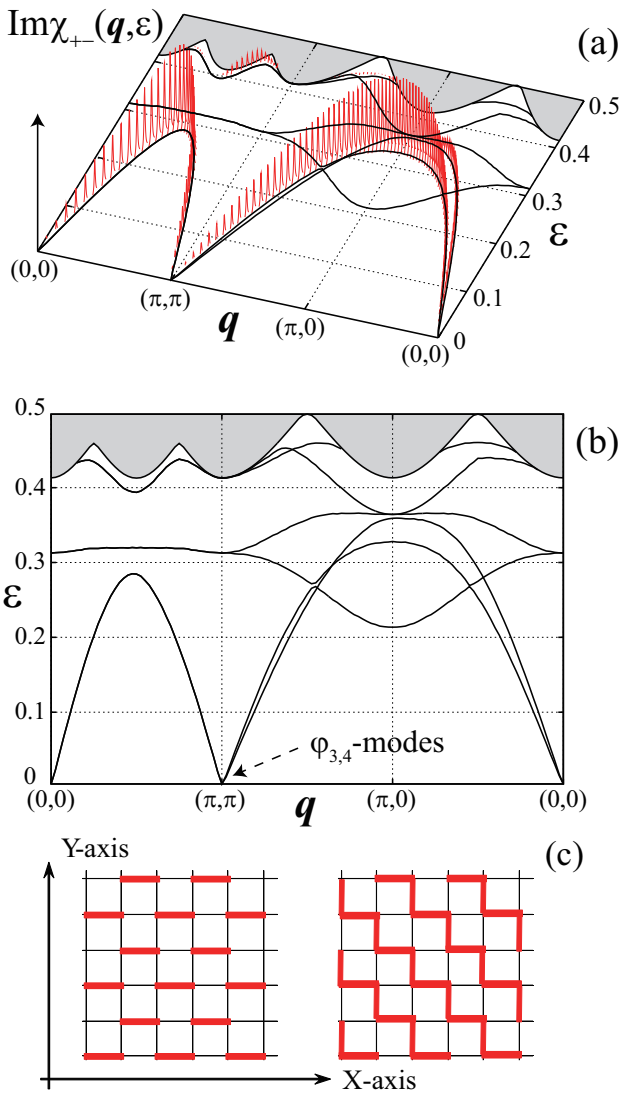

FIG. 8: (Color online) Dynamical structure factor $\mathrm{Im}\chi_{+-}(\boldsymbol{q},\epsilon)$ at the zero temperature at the critical point $J_2/J_1 = J_{c,2} = 1.0448$. The grey regions denote Stoner continuum. (a) Spectral wight of the collective modes in $\mathrm{Im}\chi_{+-}(\boldsymbol{q},\epsilon)$. (b) The dispersion relations for the collective modes. At the (π,π)-point, two collective modes become gapless, only to condense at $J_2/J_1 \le J_{c,2}$. (c) Staggered triplet-dimer state (left) and stripe-like order (right).

D. Transition to the π-flux states

When the antiferromagnetic exchange J_2 increases, the spin-triplet pairing field D gets smaller, while the other two remains almost constant. At $J_2/J_1 \geq J_{c,1} \simeq 1.325$, the saddle point solution suggests that $D = 0$ and $\chi = \eta \neq 0$, where the Stoner excitations become gapless at five (inequivalent) symmetric momentum points, i.e. $(0,0)$, $(\pi/2,\pi/2)$, (π,π), $(\pi,0)$ and $(0,\pi)$. Correspondingly, all the collective excitations and their spectral weight in the spin structure factor merge into the lower edge of the Stoner continuum, when J_2/J_1 gets closer to the critical value $J_{c,1}$ from below.

V. SUMMARY AND DISCUSSION

Using the standard large-N loop expansion, we have calculated the dynamical spin-structure factor of quantum spin nematic state in the spin-$\frac{1}{2}$ square-lattice frustrated ferromagnetic model. The saddle-point analysis in the large-N limit suggests that the 'd-wave' spin nematic state in this model is a certain kind of spin-triplet pairing states of the spinon field (neutral fermion), which can be referred to as the Z_2 planar state. The spin structure factors thus calculated have two aspects; they have both spin-liquid like character and 'spin-solid' like character. The former feature is represented by the Stoner continuum which stems from the individual excitations of gapped free spinons. Owing to the ordering of the quadrupole moments, the dynamical spin structure factors also acquire coherent peaks below this continuum, which signifies the existence of the gapless spin-wave modes. Being described as the spin-*triplet* pairing states, this state also has the so-called 'squashing' mode as its gapped collective excitations. All the gapless excitations including spin-wave modes have linear dispersions with respect to the momentum. Thus, temperature dependence of (the magnetic contributions of) the specific heat in the bond-type spin nematic ordered phase is given by a quadratic function of temperature, $C_v \sim T^2$.

Spectral weight of the spin-wave modes vanishes as a linear function of the momentum, when the momentum approaches the gapless Γ point. This behavior was also theoretically observed in the site-type spin nematic phase and presumably is a universal property of spin nematic states. Related to this behavior, Tsunetsugu and Arikawa previously calculated the temperature dependence of the longitudinal relaxation time of the nuclear magnetic resonance (NMR) in a site-type spin nematic phase.[17] To calculate the same quantity in the current bond-type spin nematic ordered phase, however, we need to estimate the 2-loop correction to the spin-spin correlation function in the present formulation. Namely, the most dominant spin-wave scattering process in the nuclear spin relaxation is usually the Raman process, in which a nuclear spin is flipped by the simultaneous occurrence of 1-magnon emission and 1-magnon absorption.[24]

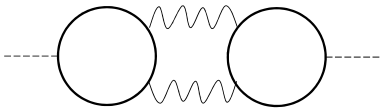

FIG. 9: Raman scattering process (2-loop level).

Such a scattering process can be schematically shown in Fig. 9, which appears at the 2-loop level of the large-N expansion. We leave this 2-loop calculation as a future open issue.[25]

The lowest gapped excitations at the (π,π)-point are identified as a certain kind of Higgs bosons, whose finite mass quantifies the stability of the Z_2 planar state against the 'confinement effect'. Though being gauge-like excitations, these massive modes comprise not only the spin-singlet pairing field but also the spin-triplet pairing fields. Owing to this triplet component, they have finite spectral weight even in the *spin* structure factor, once the momentum is deviated from the (π,π)-point: the mass can be experimentally measured in terms of the inelastic neutron scattering experiment. When these Higgs bosons lose their mass, which is the case near the ferromagnetic phase boundary,[10] a 'linear' confining potential should be introduced between neutral fermions; the state is transformed into the other phase having *no* gapped free spinons. We found that, the moment this Higgs mass vanishes, the other two gapped bosons at the (π,π)-point simultaneously change the sign of their mass from positive to negative, leading to their Bose-Einstein condensation. This condensation breaks the translational symmetry and a staggered $U(1)$ spin-rotational symmetry possessed by the Z_2 planar state, which are consistent with the 'confinement effect' in the $U(1)$ planar state.

Acknowledgments

We acknowledge Masahiro Sato, Kazutaka Takahashi, Akira Furusaki, Andrey Chubukov, Leon Balents and Kimitoshi Kono for helpful discussions. RS was partially supported by the Institute of Physical and Chemical Research (RIKEN). This work was supported by Grants-in-Aid for Scientific Research from MEXT, Japan (No. 22014016 and No. 23540397).

Appendix A: on a gapped collective mode

One of the gapped collective mode at the Γ-point is given by a linear combination of (gapless) spin-wave component and (gapped) squashing component;

$$\rho_3 = \alpha_2\big(\boldsymbol{e}_1^3 - \boldsymbol{e}_2^3\big) + \beta_2\big(\boldsymbol{e}_6^3 - \boldsymbol{e}_5^3\big). \tag{A1}$$

This mixing stems from the non-zero commutator between the spin-triplet Cooper pairing operator and spin-triplet excitonic pairing operator. Namely, when defined

on two distinct links sharing one site, these operators do not commute with each other in general,

$$\begin{aligned}\left[\hat{D}_{jl,\mu},\hat{E}_{lm,\nu}\right] &\equiv i\left[f_{j,\alpha}[\sigma_2\sigma_\mu]_{\alpha\beta}f_{l,\beta},f^\dagger_{l,\gamma}[\sigma_\nu]_{\gamma\delta}f_{m,\delta}\right]\\ &= if_{j,\alpha}[\sigma_2\sigma_\mu\sigma_\nu]_{\alpha\delta}f_{m,\delta}.\end{aligned}$$

Within the spin-wave approximation, the right hand side may be replaced by its expectation value with respect to a mean-field state. The Z_2 planar state has a finite singlet Cooper pairing amplitude on the next nearest neighbor link. Accordingly, the diagonal components of the left hand side remain finite, whenever these two triplet pairing operators are defined on the nearest neighbor x-link and y-link sharing one site;

$$\left[\hat{D}_{\langle j-x,j\rangle,\nu},\hat{E}_{\langle j,j+y\rangle,\nu}\right]=i\langle f_{j-x,\alpha}[\sigma_2]_{\alpha\beta}f_{j+y,\beta}\rangle\equiv\eta \quad \text{(A2)}$$

Due to this commutation relation, the RPA propagator at the Γ-point has a finite coupling between the in-plane spin-wave component, $\mathrm{Re}D_-\equiv\mathrm{Re}D_{x,2}-\mathrm{Re}D_{y,1}$, and in-plane squashing component, $\mathrm{Im}E_-\equiv\mathrm{Im}E_{x,1}-\mathrm{Im}E_{y,2}$;

$$[\mathcal{S}^{(2)}_{33}(0,i\epsilon_n)]=\begin{array}{c} \\ \mathrm{Re}D_- \\ \\ \mathrm{Im}E_- \\ \\ \end{array}\begin{array}{c}\begin{array}{ccccc}\mathrm{Re}D_- & & & \mathrm{Im}E_- & \end{array}\\ \begin{pmatrix}\ddots & \mathbf{0} & \ddots & \mathbf{0} & \ddots\\ \mathbf{0} & f_1 & \mathbf{0} & -ig & \mathbf{0}\\ \ddots & \mathbf{0} & \ddots & \mathbf{0} & \ddots\\ \mathbf{0} & ig & \mathbf{0} & f_2 & \mathbf{0}\\ \ddots & \mathbf{0} & \ddots & \mathbf{0} & \ddots\end{pmatrix}\end{array} \quad \text{(A3)}$$

In fact, their off-diagonal matrix element ig is linear in the Matsubara frequency $i\epsilon_n$ and linear in η;

$$\begin{aligned}f_1 &= \frac{J_1^2}{8}\frac{1}{N_\Lambda}\sum_k\frac{s_x^2}{\Delta_k}\frac{\epsilon_n^2}{\epsilon_n^2+4\Delta_k^2},\\ f_2 &= f_1+\frac{J_1^2}{4}\frac{1}{N_\Lambda}\sum_k\frac{s_y^2}{\Delta_k}\frac{J_1^2D^2s_x^2+J_2^2\chi^2c_x^2c_y^2}{\epsilon_n^2+4\Delta_k^2},\\ g &= \frac{J_1^2}{4}\frac{1}{N_\Lambda}\sum_k\frac{J_2\eta\, s_x^2s_y^2}{\Delta_k}\frac{i\epsilon_n}{\epsilon_n^2+4\Delta_k^2}\end{aligned}$$

Owing to the point group symmetry of the mean-field state, these two components do not couple with other pairing fields at the Γ-point. Replacing $i\epsilon_n$ by $\epsilon+i\delta$, one can readily see that one of the two eigenvalues is for the gapless spin-wave mode, while the other corresponds to the gapped collective mode;

$$\lambda_\pm=\frac{f_2}{2}+f_1\pm\sqrt{\frac{f_2^2}{4}+g^2}, \quad \text{(A4)}$$

The latter mode is nothing but the ρ_3-mode defined in Eq. (A1), where α_2 is linear in η.

[1] L. Balents, Nature **464**, 199 (2010); P. A. Lee, Science **321**, 1306 (2008).
[2] P. Fazekas and P. W. Anderson, Philos. Mag. **30**, 423 (1974); P. W. Anderson, Science **235**, 1196 (1987).
[3] X. G. Wen, *Quantum Field Theory of Many-Body systems* (Oxford University Press, Cambridge 2003).
[4] E. Fradkin, *Field Theories of Condensed Matter Systems*, (Addison-Wesley, 1991).
[5] A. F. Andreev and A. Grishchuk, Sov. Phys. LETP **60**, 267 (1984).
[6] P. Chandra and P. Coleman, Phys. Rev. Lett. **66**, 100 (1991); P. Chandra, P. Coleman and A. I. Larkin, J. Phys. Condens. Matter **2**, 7933 (1990).
[7] A. V. Chubukov, Phys. Rev. B **44**, 4693 (1991).
[8] T. Momoi and N. Shannon, Prog. Theor. Phys. Suppl. **159**, 72 (2005).
[9] N. Shannon, T. Momoi and P. Sindzingre, Pys. Rev. Lett. **96**, 027213 (2006).
[10] R. Shindou and T. Momoi, Phys. Rev. B **80**, 064410 (2009).
[11] M. E. Zhitomirsky and H. Tsunetsugu, Europhys. Lett. **91**, 37001 (2010).
[12] This state was refered to as a two-dimensional anolog of the Balian-Werthamer state in Ref. 10, but it is usually called the planar state in the context of superfluid ^{3}He. We adopt the name "planar state" in this paper.
[13] R. Shindou, S. Yunoki and T. Momoi, Phys. Rev. B, *in press*; arXiv:1106.5333.
[14] J. Richter, R. Darradi, J. Schulenburg, D. J. J. Farnell, and H. Rosner, Phys. Rev. B **81**, 174429 (2010).
[15] A. Auerbach, *Interacting electrons and Quantum Magnetism* (Springer-Verlag, New York 1994).
[16] C. Herring, *Magnetism IV*, editted by G. T. Rado and H. Suhl, (Academic Press, 1966).
[17] H. Tsunetsugu and M. Arikawa, J. Phys. Soc. Jpn. **75**, 083701 (2006); Journal of Physics Condensed Matter, **19**, 145248 (2007).
[18] A. Lauchli, F. Mila and K. Penc, Phys. Rev. Lett. **97**, 087205 (2006).
[19] X. G. Wen, Phys. Rev. B **44**, 2664 (1991); C. Mudry and E. Fradkin, Phys. Rev. B **49**, 5200 (1994).
[20] V. N. Popov, *Functional integrals and collective excitations* (Cambridge University Press, New York, 1999) ; D. Vollhardt and P. Wolfle, *The Superfluids Phases of Helium 3* (Taylor & Francis, 1990) and reference therein.
[21] W. P. Halperin and E. Varoquaux, *Helium Three* (Elsevier, Amsterdam 1990).
[22] A. M. Polyakov, Nucl. Phys. B **120**, 429 (1977).
[23] N. Read and S. Sachdev, Phys. Rev. Lett. **62**, 1694 (1989); Phys. Rev. B **42**, 4568 (1990).
[24] T. Moriya, Prog. Theor. Phys. **16**, 23 (1956).
[25] R. Shindou and T. Momoi, unpublished.